NUMERICAL INVESTIGATION OF PIPE UMBRELLA ROOF SUPPORT SYSTEMS IN UNDERGROUND COAL MINING

by

Forrest Paul Schumacher

A thesis submitted to the faculty of
The University of Utah
in partial fulfillment of the requirements for the degree of

Master of Science

Department of Mining Engineering

The University of Utah

August 2012

Copyright © Forrest Paul Schumacher 2012

All Rights Reserved

The University of Utah Graduate School

STATEMENT OF THESIS APPROVAL

The thesis of **Forrest Paul Schumacher**

has been approved by the following supervisory committee members:

Eunhye Kim	, Chair	**04/27/2012** Date Approved
Michael G. Nelson	, Member	**04/27/2012** Date Approved
Daniel J. Brunner	, Member	**04/27/2012** Date Approved

and by **Michael G. Nelson** , Chair of

the Department of **Mining Engineering**

and by Charles A. Wight, Dean of The Graduate School.

ABSTRACT

Weak roof conditions in underground coal mines are a common occurrence and cause significant problems in delaying production. Thus, mine operators must look into additional support methods that reinforce the commonly used bolting, trussing, and cribbing methods. The work presented in this paper conceptualizes and models two methods of pipe umbrella roof support methods intended for employment in the underground coal mining environment. The first system is a pipe umbrella over a single entry of a development section. Secondly, a double layered pipe umbrella mesh is proposed as a reinforced roof over a longwall recovery room. Boreholes for such a configuration as the second system require precision placement and current state of the art technologies in horizontal directional drilling must be utilized.

The design methodology was evaluated by examining a case study of a western U.S. coal mine and its specific geologic conditions. Geotechnical laboratory testing was performed for a weak sandstone channel material that occurs in large extents at the mine for input into numerical models. Two and three-dimensional finite difference models in Fast Lagrangian Analysis of Continua (FLAC) were developed and used as tools in the design of the pipe umbrella roof support methods proposed. One method utilizes beam elements embedded in the continuum model, while the other uses an equivalent modulus approach for modeling the reinforced zone. The effectiveness of a carefully designed pipe umbrella system is controlled by the pipe spacing, strength of the steel, and the structural

geometry of the pipe. Numerical modeling of the reinforced roof shows that a reduction in recovery room closure can be achieved for the safe extraction of longwall support shields.

TABLE OF CONTENTS

LIST OF FIGURES

Figure Page

LIST OF TABLES

ACKNOWLEDGEMENTS

Any piece of technical literature is written as a combined effort between those researching/writing a document for a particular problem and those providing invaluable advice on approaching the problem. I would like to express my sincere appreciation and gratitude to all of those who contributed to the completion of my thesis. This includes anyone who provided advice, guidance, and assistance towards gathering, making sense of, and presenting the information logically.

I wish to express my appreciation to my advisor, Eunhye Kim, who provided technical advice, numerical modeling expertise, and overall suggestions on putting together a successful thesis. I would also like to thank my other committee members: Daniel J. Brunner, whose expertise in directional drilling and practical experience in the mining industry served invaluable to the completion of my research, and Michael G. Nelson, who greatly helped put my research focus on the right path.

I would like to thank all of the staff in University of Utah Mining Engineering Department for assisting in my exceptional educational experience. Special thanks to Rob Byrnes and Kim McCarter, who graciously helped me with the preparation and testing of material in the rock mechanics laboratory.

Special thanks are also given to the staff at REI Drilling for sparking my interest in the countless applications of horizontal directional drilling in the mining industry.

Excellent supervision and support was given to me by REI Drilling, as they provided me the opportunity to complete my graduate work under their scholarship and support.

Furthermore, I would like to thank my family for their belief in me and sticking together through the many moves across the country to various small mining towns. Without the support of my father and him having a profession as a mining engineer, I would never have been introduced to the mining industry and the many interesting topics that it holds.

Finally, I wish to thank my wife, Nicole, for her love and full support in all aspects of my life

1 INTRODUCTION

At an underground coal mine in the western U.S., ground control problems and roof falls have occurred in areas where the geological formation in the mine roof consists of a water saturated sandstone unit. This sandstone unit occurs in channels or washouts, due to the depositional environment of the coal and strata beds. It is quite common for the mine operation to encounter these sandstone channels during normal operation. Roof falls are prone to occur in the development sections under the sandstone channel material; however, the most problematic situation in the mine operation is when the longwall recovery room is located directly beneath the sandstone channel.

Many coal mines have weak strata in the immediate roof that cause problems and delay production. Sometimes the use of only the usual roof support methods such as roof bolting and meshing is not enough to prevent major roof falls from occurring in an uncontrollable fashion. Thus, mine operators must look into additional support methods which reinforce current practices. Additional support methods include injection grouting, steel sets, and variations of pipe umbrella systems as employed in tunneling operations. These additional support methods would not, however, be widely used throughout the normal coal mining process. Rather, reinforced ground and pre support methods, such as pipe umbrella systems, would be installed in problem areas that have been targeted through geological projections in advance of undermining.

The research presented in this paper discusses and proposes two systems of supplementary roof control as a case study for a particular western U.S. coal mine. System 1 is a single row of horizontal steel pipes installed perpendicular to a mine headgate axis and above the current roof support. The proposed method of roof support can be installed in such a way that it does not interfere with development operations from an adjacent entry or travel way. System 2 is a method of roof support that adds additional support measures for a longwall recovery room. A double layered pipe umbrella system is proposed to be installed as pre-support, passive roof support that effectively stiffens the immediate roof above, allowing the shield recovery process to occur under lessened stress conditions over the excavation. Thus, displacements in the mine roof are minimized, allowing for reduced squeezing action of the longwall shields during recovery.

Laboratory tests were performed on a particular weak sandstone from a western U.S. coal mine. Unconfined compressive strength (UCS), tensile strength, and Young's Modulus were found though testing performed at the University of Utah. Fourteen samples were prepared and tested for the determination of the unconfined compressive strength and Young's Modulus. Thirty-two samples were prepared and tested for tensile strength using the popular Brazilian test. Results of the laboratory testing showed consistency with historical geotechnical data of the same formation.

Numerical modeling with the commercial finite difference software packages FLAC 2D and FLAC 3D was performed for three separate models. The first model is a two-dimensional model of System 1 and simulates the excavation of a typical three entry gate road section in the western U.S. coal mine. Beam elements were installed in the

model above one of the mine entries and the spacing was varied in the out-of-plane direction along with the geometric parameters. The purpose of this model was to determine the bending stress in a pipe umbrella due to undermining. The second model is a three-dimensional simulation of System 1 and is of a single entry with embedded beam elements in the mine roof. Results for the safety factor of the beams in first and second models are compared against an analytical calculation of a beam in bending with a uniformly distributed load.

An analysis of a pipe umbrella roof support design was performed based on the results of the numerical modeling. Beam elements in FLAC 2D and 3D undergo bending due to undermining and develop moments. Using well-known beam bending formulae, a factor of safety was determined for various configurations of an umbrella pipe system over a single coal mine entry.

The third model is a three-dimensional simulation of a longwall recovery room as mining approaches the end of a panel for System 2. A reinforced zone was installed in the immediate roof above the recovery room and the stresses and displacements were monitored. The results show that a relative increase in stiffness of about 185% for a reinforced zone reduce the displacements in the longwall recovery room roof by approximately 0.125 m. This is a substantial amount, as it pertains to such a small area in a very large numerical model. A reduction in roof displacement after longwall shield recovery is extremely beneficial to mine operators who struggle with delay during this process.

Geotechnical conditions of a particular western U.S. mine are assumed in all of the analyses. Material properties from laboratory testing performed at the University of Utah

and other sources were used in the numerical models. Although this research is focused on a specific western U.S. mine, the methods proposed in this paper can be applied to coal mines in general. The research in this paper shows that pipe umbrella systems can be utilized in the coal mine setting where weak roof conditions exist. The effectiveness of a carefully designed pipe umbrella system is controlled by the pipe spacing, strength of the steel, and the structural geometry of the pipe. A series of design plots are provided herin that show the factor of safety of the umbrella pipes in bending vs. their spacing along the axis of the coal mine entry.

2 LITERATURE REVIEW

2.1 Geology of the Mine

The coal field of interest is located on the north-eastern flank of the Rock Springs Uplift, which is a north-south trending asymmetrical anticline structure. This anticline separated the Green River Basin, to the west, from the Great Divide and Washakie Basins to the east. The coal deposits occur within the Deadman Coal Zone that lies in the lowermost portion of the Fort Union Formation and is of Paleocene age (56-65 million years). The Fort Union Formation has a widespread aerial distribution and is exposed in portions of Colorado, Wyoming, Montana, North Dakota, and South Dakota. In the immediate mine area, the major strata are composed of thin to massively bedded, fine-grained, well-sorted sandstones interbedded with siltstones, claystones, thin discontinuous carbon stringers, and sub-bituminous coals (NERCO 1981).

There are five identified economically mineable coal seams within the mine's coal deposit. They are designated in descending order, D-5 through D-1. The Deadman Coal Zone is currently being mined with surface techniques and underground longwall mining. Within the permitted mining area, the coal seams show a bifurcating geometry which results in coal seam splitting, thin individual coal seams, and fluctuating inter-burden thicknesses. The focus of this study will be on the underground longwall mine, which is currently mining the D-41 seam. The D-41 seam is approximately 4 m thick and is comprised of seams D-1 through D-4 joining together to form a mineable seam. The

strata associated with the coal deposit vary laterally and vertically. The strata are relatively un-deformed and dip from 2° to 5° at approximately N 45° east. There are large normal faults evident that have displacements ranging from 9 m to 76 m vertically. Figure 2.1 shows a generalized cross section of the coal seam structure and orientation.

Sandstone channels exist periodically throughout the Deadman Coal Zone, which are very weak and water saturated units. Normally, a sandstone channel unit extends from the immediate roof contact to an overlying coal seam that is approximately 15 m to 20 m above the mined coal seam. This sandstone is a very weak unit, where laboratory (intact rock) compressive and tensile strengths are approximately 11 MPa and 0.52 MPa respectively. A pre-support technique would be preferable in this type of situation as a preventative method for major roof falls. Therefore, a methodology for the design and installation of a pipe umbrella system is studied in this paper on a site specific basis.

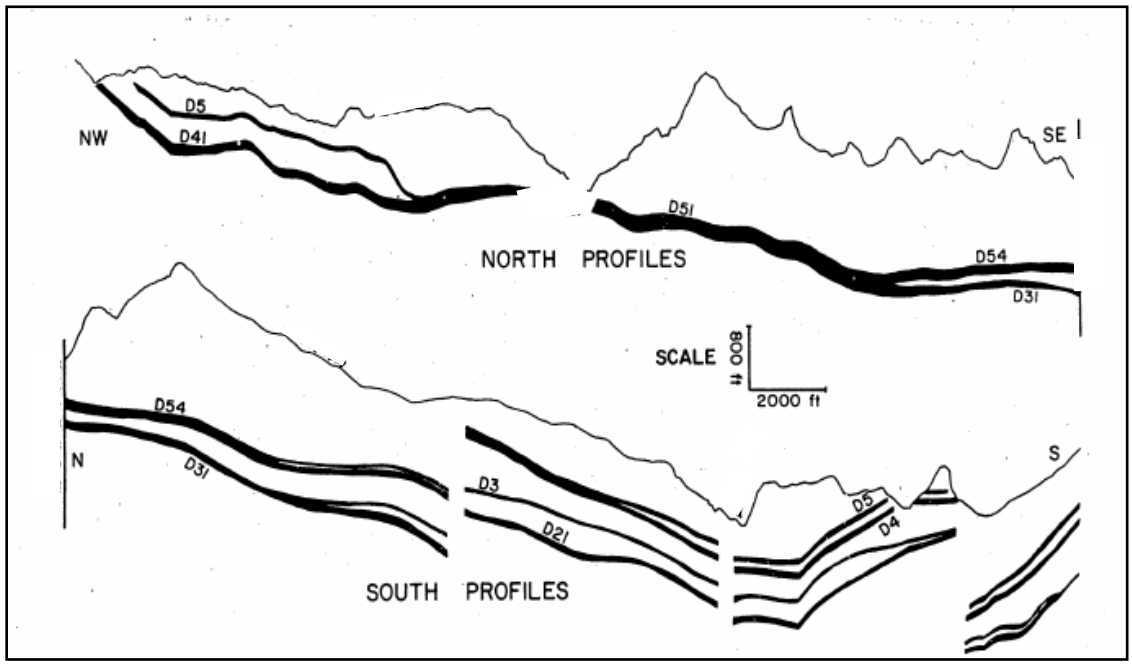

FIGURE 2.1 Coal seam structure at the western U.S. coal mine

2.2 Geotechnical Data

Current and historical analyses of the geotechnical properties of formations at the mine were made available by the western U.S. coal mine. Core logging and geotechnical testing report that the formations in the mining area are considered weak rock. However, the sandstone channel material, which is the major material being studied, is a very massive formation. The RQD of this rock mass has been approximated as 98. This material would be considered a massive weak formation. A combined summary of the rock properties from two geotechnical studies performed in 2001 and 2003 is presented below in Table 2.1.

From a separate study focusing on the channel sandstone material in 2011, tensile strength, unconfined compressive strength, and triaxial compressive strength tests were performed. Samples in this sequence of testing were on depths (from surface elevation) ranging from 102 m to 133 m. Note that samples in this depth interval were of the same channel sand formation. The average results from the testing performed in 2011 are shown in Table 2.2.

TABLE 2.1 Summary of rock properties from geotechnical studies performed in 2001 and 2003 (Maleki 2003)

Material	Unconfined Compressive Strength (MPa)	Cohesion (MPa)	Angle of Internal Friction (degrees)
D41 Coal Seam	11.45	2.59	50
Mudstone	18.62	5.03	34
Siltstone	25.23	6.41	36
Sandstone	21.37	6.48	28

TABLE 2.2 Results of geotechnical testing performed on channel sandstone (TerraTek 2011)

Test Type	Result
Tensile Strength (MPa)	1.04
Unconfined Compressive Strength (MPa)	18.27
Elastic Modulus (MPa)	2,237.79
Confined, 3.45 MPa, Compressive Strength (MPa)	38.24
Poisson's Ratio	0.28

2.3 Rock Mass Strength

Following Hoek et al. (2002), the Hoek-Brown rock mass failure criterion can be used to scale laboratory rock strength measurements and determine appropriate in-situ rock mass strengths. The calculations for determining equivalent Mohr-Coulomb material properties (φ and c) are shown in this section. The Hoek-Brown (HB) failure criterion, in its original form may be stated as:

$$\sigma_1 = \sigma_3 + \sqrt{a\sigma_3 + b^2} \tag{2.1}$$

where, a and b are strength properties of the material; σ_1 and σ_3 are major and minor principal stresses, respectively. This criterion is nonlinear in terms of σ_1 and σ_3. The strength parameters of a and b can be expressed in terms of the unconfined compressive strength and the tensile strength of the material as the following:

$$a = \frac{C_0^2 - T_0^2}{T_0} \tag{2.2}$$

$$b = C_0 \tag{2.3}$$

The above function for the HB failure criterion is representative of the strength of intact rock under a controlled setting, such as, laboratory tests on strength. However, the strength of a rock mass is only a fraction of the intact rock strength. This means that the Hoek-Brown failure criterion must take into account the discontinuities and weathering of the rock mass. This is typically taken into account based on the rock type and rock mass quality, which is quantified by the Geological Strength Index (GSI). Thus, the Hoek-Brown failure criterion for a rock mass can be written as:

$$\sigma_1 = \sigma_3 + \sigma_{ci}\left(m_b \frac{\sigma_3}{\sigma_{ci}} + s\right)^a \tag{2.4}$$

where σ_1 and σ_3 are the maximum and minimum principal stresses, respectively, m_b is the value of the Hoek-Brown constant for the rock mass, *s* and *a* are constants that depend on the characteristics of the rock mass, and σ_{ci} is the unconfined compressive strength of the intact rock pieces. Note that if *s*=1 and *m* is some variation of the intact rock tensile strength and compressive strength, the original form of the HB failure criterion for the intact rock can be written as:

$$\sigma_1 = \sigma_3 + \sigma_{ci}\left(m_i \frac{\sigma_3}{\sigma_{ci}} + 1\right)^{0.5} \tag{2.5}$$

where m_i is the constant calculated from the intact rock strength. With respect to the GSI value of the rock mass, the coefficients m_b, *s*, and *a* can be directly calculated with the following equations (for GSI > 25):

$$m_b = m_i e^{\frac{GSI-100}{28}} \quad (2.6)$$

$$s = e^{\frac{GSI-100}{9}} \quad (2.7)$$

$$a = 0.5 \quad (2.8)$$

While the Hoek-Brown criterion is useful in its own nature, a methodology has been developed to obtain equivalent Mohr-Coulomb parameters by fitting an average linear relationship to the curve generated by the Hoek-Brown equation. This method is particularly useful because most numerical modeling software packages operate on the well accepted Mohr-Coulomb failure criterion. Unlike the Hoek-Brown failure criterion, the Mohr-Coulomb criterion operates on an internal friction angle (φ) and cohesion (c). The Mohr-Coulomb failure criterion may be expressed in terms of major and minor principal stresses as the following (Pariseau 2006):

$$\left|\frac{\sigma_1-\sigma_3}{2}\right| = \left(\frac{\sigma_3+\sigma_3}{2}\right) sin\,\varphi + c\,cos\,\varphi \quad (2.9)$$

where σ_1 = major principal stress

σ_3 = minor principal stress

φ = internal angle of friction

c = cohesion

Derivation of the Mohr-Coulomb fit parameters is unnecessary as it is quite involved, so a simple presentation of the results will suffice. Although cumbersome

equations, the equivalent friction angle (φ) and cohesion (c) can be found using the following:

$$\varphi = \sin^{-1}\left[\frac{6am_b(s+m_b\sigma_{3n})^{a-1}}{2(1+a)(2+a)+6am_b(s+m_b\sigma_{3n})^{a-1}}\right] \quad (2.10)$$

$$c = \frac{\sigma_{ci}[(1+2a)s+(1-a)m_b\sigma_{3n}](s+m_b\sigma_{3n})^{a-1}}{(1+a)(2+a)\sqrt{1+\frac{(6am_b\sigma_{3n})^{a-1}}{(1+a)(2+a)}}} \quad (2.11)$$

where $\sigma_{3n} = \sigma_{3max}/\sigma_{ci}$. All other parameters have been defined earlier.

2.4 In-Situ Stress at the Mine

From work performed by a geotechnical service company for the mine, in-situ horizontal stresses and their directions were determined using the overcoring method. This method involves the indirect measurement of the secondary principal stresses in the horizontal plane perpendicular to a vertical core hole. For this method, a borehole is drilled vertically to a predefined depth and counter-bored so that any extra core stump left at the bottom of the hole is cleared out. Next a pilot hole is drilled an additional ~0.5 m and a strain measurement device is lowered into the pilot hole and bonded to the borehole wall. This assembly is then over-cored and removed from the bottom of the hole, which causes a release of stress in the over-cored material; the strain magnitudes and directions that this material undergoes are measured. From these data, the horizontal stresses can be calculated (NSA Geotechnical Services Inc. 2003).

The major and minor principal stresses in the horizontal plane can be expressed in terms of the mean effective stress (σ_m) and the deviatoric stress (σ_d) as follows:

$$\sigma_1 = \sigma_m + \sigma_d \quad (2.12)$$

$$\sigma_1 = \sigma_m - \sigma_d \quad (2.13)$$

The vertical stress (σ_v) can be calculated based on the specific weight (γ) of the overburden and the depth (h) with the following formula:

$$\sigma_v = \gamma h \quad (2.14)$$

Assuming elasticity, and that the rock at depth is laterally constrained so that there is no allowable strain in the horizontal direction, the horizontal stress due to self-loading following Poisson's effect is:

$$\sigma_h = \sigma_v \frac{\nu}{1-\nu} \quad (2.15)$$

where ν = Poisson's ratio.

The remaining component of the total horizontal stress is the stress caused by tectonic forces in the earth. Horizontal stresses in a material at some depth in the earth will vary by its elastic modulus, E. The major and minor principal stresses in the horizontal plane (σ_{1h} and σ_{2h}) are therefore represented by the following set of equations:

$$\sigma_{1h} = \sigma_h + E\frac{\varepsilon_{1tec} + \nu\varepsilon_{2tec}}{1-\nu^2} \quad (2.16)$$

$$\sigma_{2h} = \sigma_h + E\frac{\varepsilon_{2tec} + \nu\varepsilon_{1tec}}{1-\nu^2} \quad (2.17)$$

where, ε_{1tec} and ε_{2tec} are the strains measured by the over-coring method and E is the elastic modulus of the material.

A series of seven over-cores were taken at the mine at depths close to the mining level. The orientations of the principal stresses in the horizontal plane were calculated to be N 40° W for the major principal stress and N 50° E for the minor principal stress. At depth, the average magnitudes of the tectonic stress components were found to be 2.07 MPa and 1.31 MPa for major and minor tectonic stresses respectively (NSA Geotechnical Services, Inc. 2003). Therefore, the total major and minor principal stresses at depth for the mine can be calculated using the following formulas:

$$\sigma_{1h} = \sigma_h + 2.07 \text{ (MPa)} \quad (2.18)$$

$$\sigma_{2h} = \sigma_h + 1.31 \text{ (MPa)} \quad (2.19)$$

Esterhuizen et al. (2009) recommend that pre-mining horizontal stress can be calculated in each layer of rock based on its elastic modulus and the vertical stress due to gravity loading. The following equations are suggested to be used to calculate the maximum (σ_{h1}) and minimum (σ_{h2}) horizontal stress components in units of MPa:

$$\sigma_{h1} = 1.2\sigma_v + 2.6 + 0.003E \quad (2.20)$$

$$\sigma_{h2} = 1.2\sigma_v + 0.0015E \quad (2.21)$$

where E = elastic modulus

σ_v = vertical overburden stress.

2.5 Pipe Umbrella System in Tunneling

The pipe umbrella support system, also known as the fore pole or spiling method, is commonly used in tunneling operations where ground conditions are very poor and ground settlement above the tunnel needs to be minimized. Pipe umbrellas serve as a method of pre-support in underground excavations to increase stability in the working area and decrease the deformations due to construction. In tunneling, a pipe umbrella support system consists of steel pipes that are installed from the current working face out to a distance on the range of 12 m to 15 m in front of the face advance. The pattern of pipes is arranged in a manner so that it outlines the tunnel extents. Diameters of the pipes range from 70 mm to 200 mm (Volkman et al. 2008). Figure 2.2 depicts an installed pipe umbrella support system installed for a single tunnel. The effectiveness of the umbrella pipes comes from the redistribution of face stresses in the longitudinal direction. Each pipe transfers the loads from the supported areas to the less critical areas, which are used as abutments (Volkman et al. 2008).

There are two available installation methods for pipe umbrellas: predrilling method and cased drilling method. The predrilling method is characterized by a three-step installation process. First, a horizontal borehole is drilled to the desired location and then in a second step, the pipe is pushed into the predrilled hole. The borehole is then often pumped full of grout.

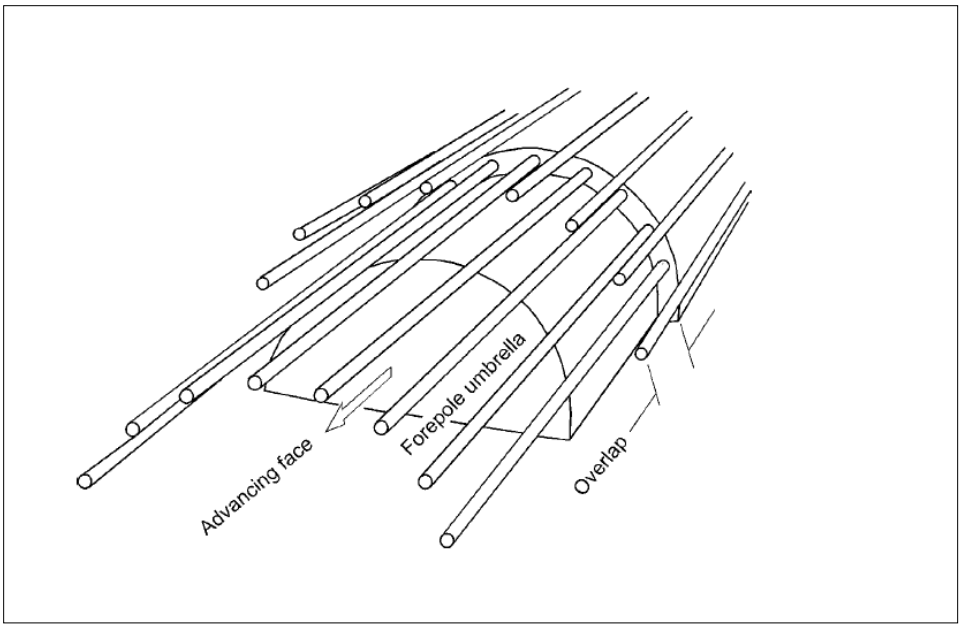

FIGURE 2.2. Depiction of pipe umbrella support system as used in tunneling

The predrilling method is often employed by operations that do not have drilling equipment specifically made for the installation of pipe umbrellas. The pre-drilled method is generally not the desired choice, because of the instability of an open borehole under high stress conditions. The borehole also must be drilled to a larger diameter than the installed casing so that it can easily be installed. Thus, the annulus between the pipe and the borehole wall must be filled with more grout, relative to the other installation method.

The cased-drilling method involves using only two steps for final installation. Using this method, the umbrella pipe follows directly behind the drill bit and stays in place after completing the borehole. Drilling crews can install this type of system by using conventional jumbos. Time is decreased from the predrilled method and the borehole is never left open.

In a methodology proposed by Hoek (2000), the analysis of this type of support can be numerically modeled though the use of an equivalent strength of the reinforced zone. This assumes that a process of weighted averages can be used to estimate the strength and deformation of the zone of reinforced rock. Figure 2.3 depicts this approach and how an equivalent elastic modulus may be calculated for a 'three phase' composite reinforced area of rock. It is also possible to use numerical tools to model a pipe umbrella system using structural beam elements within a finite element or finite difference grid. Elements can be coupled to grid points within the model, become subject to loads due to excavation, and simulate bending resistance and develop moments within the structure. This type of embedded beam analysis would allow a finite element or finite difference grid to deform the beams within it (Yeo et al. 2009). One could then look at the bending moments that develop in the beam elements and analyze various beam configurations based on pipe geometry, steel strength, and bending stresses.

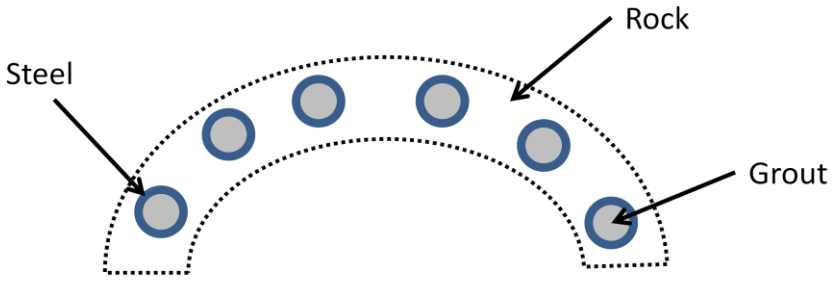

$$E_{eq} = \frac{E_{steel}A_{steel} + E_{grout}A_{grout} + E_{rock}A_{rock}}{A_{total}}$$

E = elastic modulus
A = contributing area

FIGURE 2.3 Equivalent modulus for a reinforced zone of umbrella pipes

This methodology of pre support is applicable in the coal mining industry, when areas of weak ground are encountered. One challenge of implementing this type of reinforcement in a coal mine is the geometry at which the boreholes for pipe installation must be drilled. This would be a type of pre-support that is only utilized in problem areas of a mine opening or where problem areas are predicted. Excavation methods differ from tunneling, so boreholes would need to be drilled from an adjacent entry with a much greater borehole length. This would make navigation of the borehole more difficult, but still very possible if directional drilling capabilities are utilized.

Another challenge is determining acceptable design criteria, especially when most coal mine excavations are temporary and need not be stable for long periods of time, relatively speaking. The research discussed further in this paper utilizes both methods (equivalent reinforced zone strength and embedded beam elements) for modeling a reinforced rock zone with umbrella pipes.

2.6 Modeling Pipe Umbrella System

Following Yeo et al. (2009), a pipe umbrella system was modeled in the finite element software ABAQUS in three dimensions. This was a site specific investigation on the Fort Canning Tunnel in Singapore. The tunnel length, width, and height are approximately 350 m, 15 m, and 11 m, respectively. The depth of cover is very shallow, varying from 3 m to 9 m of soil. Therefore, surface settlement needed to be minimized at a high level and a pipe umbrella system was chosen as a method of additional support. The steel pipes were modeled as beam elements tied to nodes in the finite element mesh and aligned horizontally. The beam elements were fully tied to the solid elements, so any sliding between beam and solid elements was not modeled.

There is a noticeable difference in the surface settlement in the numerical modeling results between the model with and without the embedded beam element umbrella. Vertical displacement on the surface is shown to be approximately -0.08 m and -0.10 m for beam elements and no beam elements, respectively. Yeo et al. noted that this is a striking difference given that the unsupported length is only 1 m between the tunnel lining and the working face.

2.7 Why Simple Models Geomechanics

Hammah et al. (2009) describe that in the field of geomechanics and geotechnical engineering, numerical models are used increasingly to aid in the design and for decision making of underground excavations in mining. With increased computing power, modelers have been able to increase the size and complexity of models to better simulate what is happening in the real world. However, the more complex a model becomes, the more likely that the solution to the model becomes more exact and in mining geomechanics, exactness is generally not achievable. By definition, models are incomplete representations of the real world, and if a model were to incorporate every aspect of the real world, it would no longer be a model (Hammah et al. 2009).

Mining is performed in the geological environment, which provides a large amount of uncertainty. Therefore, approximate inputs in a model will yield approximate outputs; it is better to be approximately correct than be precisely incorrect. According to Hammah et al. (2009), we can accomplish the following with a numerical model:

1. Development of understanding of the phenomena
2. Formulate the proper questions

3. Reasonable approximation of the behavior of a geological system and make meaningful predictions of an outcome under various conditions.
4. Aid in the design of solutions and decision making.

The important first step of any geomechanical model is the careful consideration of the overall goals of the modeling exercise. The next step is to define overall model boundaries, material properties, and the simplicity of the model. Depending on the modeling goal, it is worthwhile to simplify the model as much as possible. This may be something such as only modeling half of a circular tunnel due to symmetry, selecting a representative cross section and moving from three dimensions to two dimensions, or assuming a single material property that accurately represents a group of materials. If a numerical stress analysis design tool is used properly, the model will demonstrate the ability to accurately capture key elements of the geologic site model. The model must accurately simulate how these elements interact with a mine design (Larson and Wyatt 2009). A model is only valid if the results can be compared to its real world situation and the key aspects of the actual situation are evident in the numerical model.

2.8 Strain Hardening Gob Model

During the longwall mining process, the caved material behind the longwall face (gob) forms a rubble zone. As the face advances farther, the overburden subsides and re-stresses the gob material, causing it to compact. This compaction essentially is an increase in the overall stiffness of the material. The re-compaction of the gob after undermining is an important process since it can alter the pillar and abutment loads by acting as an additional support for the static system (Esterhuizen et al. 2009).

In a so-called "modulus updating" method, Badr et al. (2003) proposed that the gob compaction process can be numerically modeled as a nonlinear elastic material. The bulk modulus of the gob continually increases as a function of its vertical strain. The algorithm for this process is shown in the following formula:

$$K = \frac{1.75}{0.5 - \varepsilon_v} \text{ (MPa)} \tag{2.22}$$

where K = bulk modulus

ε_v = vertical strain

The height of the cave of the roof stratum in a longwall mine and the compaction characteristics of the broken rock within the gob have a large impact on the stresses and strains in a rock mass as the result of longwall mining. A recent study performed by Whittles et al. (2005) suggested that the height of the rubble zone in a longwall gob can be characterized by the following equation:

$$H_c = \frac{100h}{C_1 h + C_2} \tag{2.23}$$

where H_c = caving height (m)

h = mining height (m)

C_1 and C_2 = empirically derived coefficients depending on stratum lithology

2.9 Longwall Mining

It is important to those reading this paper that the longwall mining process be understood in detail. The following description of the longwall mining process is in reference to the SME Mining Engineering Handbook 2nd Edition. In longwall mining, coal or other stratified materials are removed in large underground blocks or panels. These panels are on the scale of 3,000 m long, 300 m wide, and 3 m in height and can take months to mine depending on conditions. In order to be mined with this technique, a panel of coal needs to be developed using continuous mining techniques. Continuous mining allows the coal to be mined, collected, and hauled out of the mine with minimal amounts of delay.

A typical longwall coal mine is separated into the following sections: mains, gate-roads (development sections), bleeders, and longwall panels. The mains are a series of parallel entries or tunnels separated by strings of coal pillars that create cross-cuts between the entries. In large mines, there may be as many as 12 parallel entries. Depending on the extent of the mine plan, the mains are continuously being mined so that the next panel is developed before the previous panel has been completed, minimizing chance for major delay. The mains are excavated with continuous mining techniques developed from an outcrop, shaft bottom, or slope bottom and serve as access to the development the rest of the mine. The mains also serve as the main haulage way for miners, coal, power, water, and supplies.

The gate-road sections are a series of parallel entries, typically two to four in the U.S., that are mined with the continuous mining method generally perpendicular to the mains. Like the mains, the gate-road sections are separated by strings of coal pillars that create cross-cuts between the entries. Gate-road sections can be called development

sections and they are mined to establish the extent of the length and width of a longwall panel. Typically, the headgate is the side of the longwall panel that acts as the haulage way and fresh air intake to the face of the longwall. The tailgate is the side of the longwall panel that ventilates methane and coal dust produced along the mining face to the mains and out of the mine. Since longwall panels are typically mined parallel to each other, the headgate of the current panel will normally become the tailgate section of the next panel, unless ground conditions require that a barrier pillar between longwall panels be created.

Bleeder entry development is created in a coal mine to ventilate the “gob”, or caved area behind the direction of mining. These are developed so a controlled flow of air can ventilate the gob so that gases, such as methane, will not flood the fresh air of the mine. If the mine uses progressive sealing with longwall face advance, the bleeder entries are not used. The bleeder entries establish the extent of the length of a longwall panel.

Once the panel of coal has been created, a mining machine is used to shear coal from the face starting at an entry developed across the width of the panel farthest away from the mains. As the coal is sheared from the face, it falls on to a conveyor system that stretches the entire width of the panel that moves the coal to a staging system and out of the mine. With each pass along the face, the material above the mined coal panel is left unsupported and is allowed to cave behind the mining equipment. The mine roof above the mining equipment and workers is temporarily supported by a series of hydraulic support shields that move in the direction of mining with each pass. It is ideal for the roof behind the shields to cave as quickly as possible so that the shields and immediate mining face support the least amount of abutment load generated by the extraction of material.

This method is typically referred to as retreat mining, since mining is commencing from the farthest point of the development sections inward.

2.10 Longwall Shield Recovery

Mining for coal and other minerals beneath the earth's surface can present a variety of problematic ground conditions. In longwall mining, it is necessary to move the equipment from the end of a mined out panel to the next area of mining so that the mineral can be continuously produced. In practice, this can take a significant amount of time while costing a mining company considerable amounts of money in lost production and man-hours. Much of the lost production time in a longwall move can be due to poor ground conditions and inadequately planned roof support in the longwall recovery room that does not allow for easy extraction of the support shields.

The longwall recovery room is a mined single entry developed along the width of the panel. It normally facilitates mine workers with enough space to support the mine roof and ribs with conventional methods such as bolting, cribbing, and meshing then remove the pan-line, shearing machine, and support shields. The recovery room can either be mined with a continuous miner before the longwall face reaches the location or mined with the longwall shearing machine once the specified location (end of panel) has been reached.

Conventional methods for developing a recovery room require that a pre-determined location be established and ground control preparations be made between 12 to 14 shear cuts from the extraction point. With each pass of the shearing machine, welded wire roof mesh, chain link material, or nylon woven geo-textile material is placed against the roof along the length of the panel and the shields are advanced. The last 3 m

to 4 m is then mined and the shields are not advanced so that there is sufficient area to remove the equipment and prepare the mine roof and coal face with bolting and meshing (Tadolini 2003).

One major problem that a mine faces is the large abutment stress applied to the support shields and the barrier pillar after mining has been completed. This is the main reason for the extensive roof support in the recovery room. The weight of overburden directly behind the support shields is no longer supported by the coal, since it has been removed. Therefore, this load is distributed on to the longwall shields and the adjacent barrier pillar. Although the ground is allowed to cave behind the shields and relieve some of this pressure, a significant amount of weight is placed on the longwall support shields and the barrier pillar. This condition can worsen if the surrounding rock is water saturated and very weak, or if the immediate roof does not cave easily. In certain cases, conventional methods such as bolting, cribbing, and meshing are not enough to support the roof. Conventional methods are only capable of supporting an abutment load to a certain extent up into the mine roof. If supplemental methods are used, such as a hybrid approach of the pipe umbrella support system, an increased level in the stability longwall recovery room can be achieved.

2.11 Horizontal Directional Drilling

Directional drilling is the science and art of deviating a borehole along a planned course to a subsurface target, where the location has a given lateral and/or vertical distance and direction from the collar. In the mining industry, directional drilling is used in a variety of ways. The most common uses of directional drilling in the mining industry are for delineation of old mine workings, defining geologic structure ahead of mining,

methane drainage applications, water drainage of adjacent workings, geotechnical and exploration coring, and utility purposes. Careful measurement while drilling allows for accurate placement of the drill path. Directional steering capabilities are achievable due to a bent sub located behind the drill bit. The orientation of the bent sub controls the direction of force exerted on the borehole wall, and in turn the direction of the force on the drill bit. Figure 2.4 depicts this concept.

Directional drilling motors are commonly run on the energy produced by fluid flow (drilling mud). As drilling mud is pumped at high pressures, the fluid energy is converted into rotational mechanical energy on the rotor, which in turn provides a high amount of torque and rotation speed to the drill bit. This means that the drill rods do not rotate in the borehole. Instead, drilling footage is generated by a rotation of the bit at the end of the drill string and a "sliding" of the drill rods along the borehole wall. The torque is supplied by water or drilling fluid being passed through the drill string and a helical

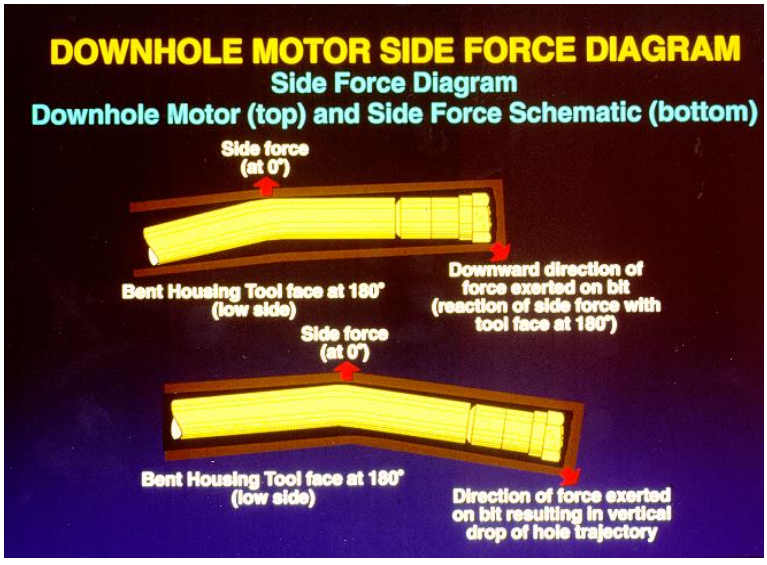

FIGURE 2.4 Downhole motor force diagram (REI Drilling 2008)

rotor system (motor) at high pressure. Depending on geological conditions, it may be desirable to have either more torque or more RPM's. These factors are dependent on the configuration of the rotor system in the motor housing and the amount of lobes and twists on the rotor. Figure 2.5 shows a cutaway photograph of the configuration of a downhole motor as used in directional drilling.

It is very important that a directional borehole is surveyed accurately during the drilling process. This gives the ability of the drill operator to steer and control the borehole along a predetermined path and identify structures or anomalies at a specific location along the drill path. In common practice, directional sensors are located down-hole, behind and in series with the drill bit and drilling motor. The sensor will commonly consist of three axes of accelerometers and three axes of magnetometers. Accelerometers measure the direction of pull of the gravity, which in turn is an indirect measure of the sensor inclination and bit roll. Magnetometers measure the strength of the earth's local magnetic field. Knowledge of the roll and inclination angles enables determination of the horizontal components of the earth's local magnetic field; this information defines the azimuth angle. Sensor data are sent to the surface with a method that is suitable for the

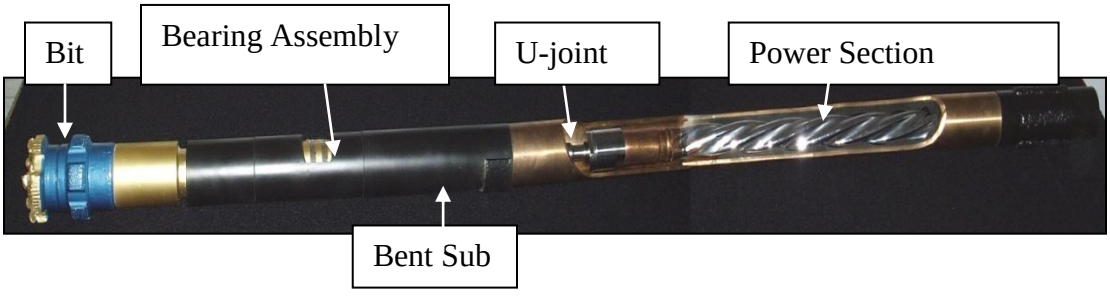

FIGURE 2.5 Configuration of a down-hole motor assembly

formation conditions. This could be electromagnetic data transmission through the geologic formation, or some type of fluid pulse telemetry through the annular drilling fluid.

In horizontal directional drilling as used in the coal industry, data from the directional sensor package are collected via a wire-line through the drill string. This data transmission method is commonly practiced in underbalanced drilling, where the pressure of the wellbore is kept at a lower pressure than the surrounding formation and there is not a continuous fluid or mud column that might allow for other types of communication such as mud pulse telemetry. Wire-line data communication can also be kept at low enough voltages so that safety regulations can be met for potentially explosive atmospheres, such as in an underground coal mine.

Recent technological advances in borehole surveying have allowed for the directional sensor to stay in-hole for the duration of drilling, as it is encased in a water tight pressure barrel. Drill rods near the bit and the pressure barrel are typically made up of a nonmagnetic Copper Beryllium alloy to reduce any magnetic interference with the directional sensor. Some directional motors are also constructed out of nonmagnetic material. Before the previously described technology was developed, surveying was done on a "single-shot" basis, where drilling ceased and the survey instrument was tripped in and out of the hole for each survey shot.

In order to determine a borehole location relative a known collar location, three properties of a borehole survey point are needed: azimuth, inclination, and drill string length (survey distance between points). There are various methods for calculating or

determining the trajectory of a borehole from the orientation data. Generally there are two groups of calculation methods: straight line approximations and curvature methods.

The Average Angle method is an example of a well path calculation based on straight line approximations between two points. The Minimum Curvature method assumes that two adjacent survey points lie on a circular arc. The arc is located on a plane and the orientation of which is defined by known inclination and directional angles at the ends of the arc and incorporates a radius factor (RF), which depends on the severity of the dogleg (Amorin et al. 2010). Figure 2.6 shows a model plan view of a directionally drilled in-seam borehole for verification of old underground workings. This type of drilling allows mine operators to verify continuity of the coal seam so that they can safely mine near abandoned mine workings.

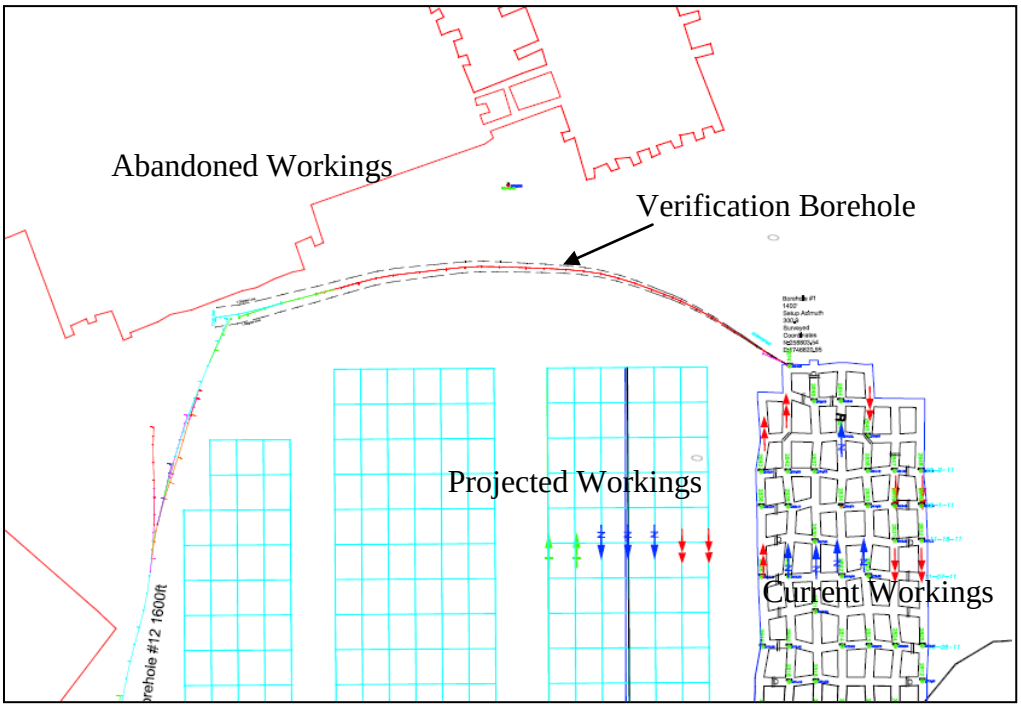

FIGURE 2.6 Plan view of a directionally drilled borehole used for the verification of coal continuity between projected and abandoned workings (REI Drilling 2012)

3 CONCEPTUAL MODEL

With the technology that encompasses current directional drilling practices, there is a potential for innovative techniques in roof support for underground excavations. Directional drilling can be used as a tool for installing supplementary roof support in underground mines. Long, steered holes can be drilled and umbrella pipes can be placed in predetermined locations before undermining has taken place. Pre-support methods, such as pipe umbrella systems can then be installed in various configurations. The example studied in this paper focuses on a two conceptual umbrella support systems using site-specific material properties and mine geometry. System 1 is a single row of umbrella pipes over a coal mine development entry. System 2 is a double layered umbrella pipe system installed over a longwall take down room, where holes are drilled and cased from an adjacent entry in advance of undermining. Concepts of each design are highlighted in this section.

3.1 System 1: Pipe Umbrella System over a Single Entry

Upon development, longwall mining, and longwall shield recovery the studied mine commonly intercepts areas where a weak sandstone channel formation occurs in the immediate roof of a development section. If weak roof conditions exist, a yield zone will develop after undermining and have the potential for catastrophic failure. To prevent additional roof failure above the currently installed roof support, umbrella pipes can be

installed above a mine entry in a designed geometry for passive support. Figure 3.1 shows a cross section of the conceptual model for a pipe umbrella over a single entry.

In the plan view, the pipes are installed along the length of a mine entry at a designed spacing. This spacing determines the effectiveness of such a support method and ability of the umbrella system to prevent roof falls from growing and extending to uncontrollable heights into the roof. The major geometrical elements of a pipe umbrella system are the height of yield zone, height of installed pipes over the mine entry, spacing between the pipes and width of the mine entry. These parameters affect the volume of rock that each pipe must support and the selection of a pipe diameter. The yield zone of a particular mine entry will vary based on the geological site conditions.

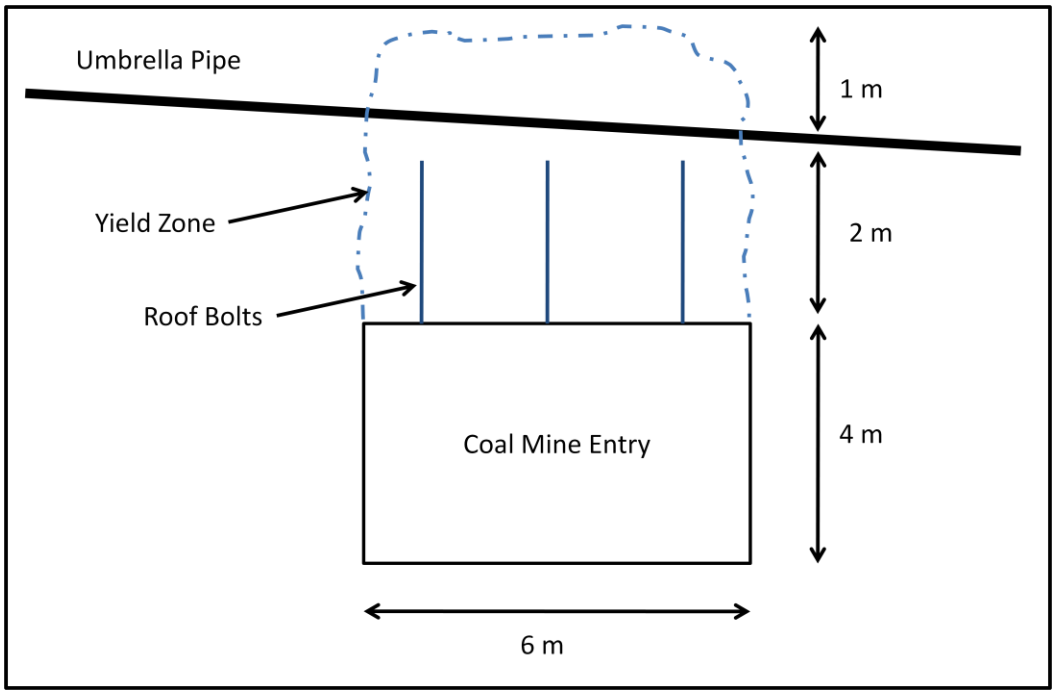

FIGURE 3.1 Conceptual model for a pipe umbrella over a single entry

Figure 3.2 shows example geometry of an installed pipe umbrella system installed over a single coal mine entry. It should be noted that for the purpose of minimizing the amount of casing/pipe material used for this method, the nonbeneficial and excess pipe can be removed and reused during the drilling process. This would be done using an inner diameter casing cutter; explanation of this process is not in the scope of this paper.

The assumption for the described case is that the roof support below the pipes fails and the umbrella system must support the weight of the material in the yield zone above the failed roof support. In this case, the pipe fan must carry a volume of rock resulting from the height of the yield zone, the width of mine entry, and the spacing between the pipes.

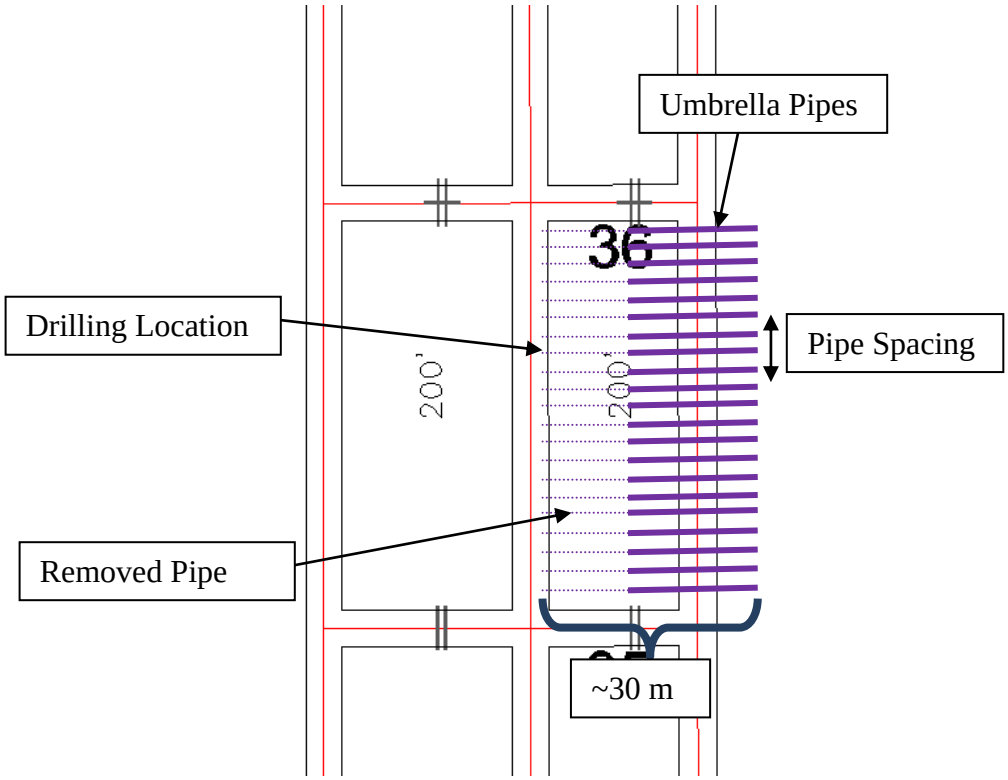

FIGURE 3.2 Plan view of the conceptual model of a pipe umbrella over a single mine entry

In the design analysis of this type of system geometry, the pipe spacing is varied along with the diameter of the pipe. In simple beam bending theory, the greater the cross sectional area of the pipe (increased diameter) the more load can be carried in the elastic limit of the steel. With an applied distributed load to each beam, a bending moment develops, and in turn a bending stress. This developed bending stress can be compared to the yield strength of the steel to find a safety factor for a given configuration.

The installation method must be taken into account when selecting a pipe diameter. Shown in Figure 3.2, the drilling length of a single pipe could be upwards of 30 m. The probability of the intersection of a deviated borehole must be minimized, therefore the smaller the pipe diameter, the better. It is easier to drill a longer borehole of smaller diameter; therefore the design recommendation is to choose the smallest pipe diameter to satisfy the design criteria.

3.2 System 2: Umbrella Pipe Mesh

An umbrella pipe mesh consists of a series of boreholes drilled at two separate elevations above the mine entry. Boreholes are drilled at an approximate 45° angle relative to the azimuth direction of the gate road section and targeted to a location above a future longwall recovery room. In the conceptual model presented, the two levels of pipes are installed at opposite azimuths from an adjacent mine entry are installed at elevations above the mine roof of 2 m and 3.5 m, respectively. Pipes are then pumped full with a grout to cement the pipes in place and increase the overall strength of the material. Figure 3.3 shows an isometric view of the general concept of the installation of a pipe mesh above a longwall recovery room. Figure 3.4 shows a generalized plan view of System 2 concept.

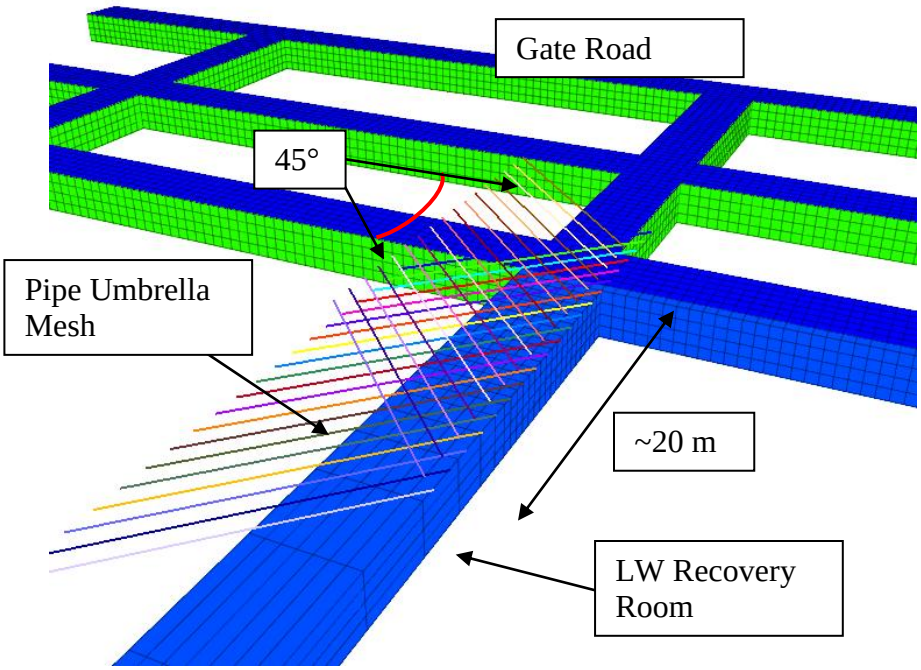

FIGURE 3.3 Conceptual isometric illustration of System 2

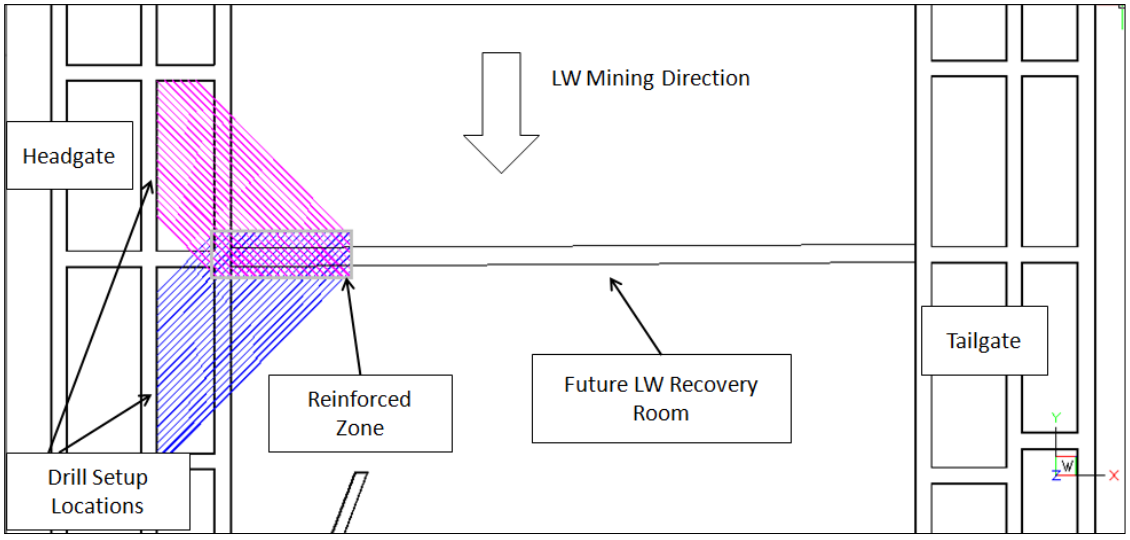

FIGURE 3.4 Plan view of the concept presented for System 2

The colored lines represent the support pipe installed in a directionally drilled borehole in Figure 3.4. The borehole originates much farther inby the borehole depth than is shown, but the general concept is depicted here. Pipes are only shown to extend to about 20 m into the longwall panel. Selection of this dimension is based on the site specific conditions of the western U.S. coal mine. It was reported that the longwall recovery process experiences the most problems between the headgate entries to about 20 m into the longwall block. It is important to note that the studied coal mine does not develop premined recovery rooms, thus a pre support method such as an umbrella pipe mesh would need to be accurately drilled and surveyed with confidence that the pipes have been placed in the proper locations.

It is not trivial how one might approach the design of this type of system. Numerical modeling seems like the logical approach so that a reinforced zone of the pipe umbrella system can be simulated to reduce displacements in the mine roof. Using the same modeling approach as used in System 1 may not be a good approach because such high abutment stresses exist in and around a longwall recovery room, that the pipes would most likely yield in any geometry if installed as beam elements explicitly. Thus, the design criteria for this type of system are the reduction of displacements in the roof of the recovery room and the redistribution of stresses to the abutment by a stiffened pipe/rock layer. Essentially, a member or zone of an equivalent stiffness can be modeled based on the weighted area modulus and strength of a steel pipe, grout, and rock mixture. The impact of the reinforced zone can be explicitly modeled and compared to the same model geometry without a reinforced zone.

3.3 Properties of Umbrella Casing

For the analysis of pipe umbrella support in a coal mine, typical pipe geometry is assumed to consist of various common drill casing dimensions. Steel casing diameters of 114 mm, 139 mm, and 168 mm were used in this study. The steel type is assumed to be high strength steel of type A514, which has an elastic modulus of 215 GPa and a yield strength of 700 MPa. Steel strength is important in the analysis of a pipe umbrella support system because the design of such a system is based on the bending stress of the steel and what range of safety factors can be achieved for various spacing of pipes and steel geometry. Assumed steel properties were taken from Hibbeler (2005). Table 3.1 shows the tabulated properties of importance used for structural analysis of a pipe umbrella system in the coal mine setting.

TABLE 3.1 Steel casing properties used in pipe umbrella analysis

	114 mm Casing	139 mm Casing	168 mm Casing
Outer Diameter (m)	0.1143	0.1397	0.168
Inner Diameter (m)	0.1017	0.127	0.143
Cross Sectional Area (m^2)	0.00214	0.00532	0.01221
Moment of Inertia (m^4)	3.127E-06	5.926E-06	1.858E-05
Steel Type	A514		
Elastic Modulus (Pa)	2.15E+11		
Yield Strength (Pa)	7.00E+08		
Polar Moment of Inertia (m^4)	6.25E-06	1.19E-05	3.715E-05

4 EXPERIMENTAL MEASUREMENTS

Laboratory measurements of the channel sandstone material from the western U.S. mine were performed to obtain Young's modulus, tensile strength, and the unconfined compressive strength. Core for the geotechnical tests was obtained directly from the mine site after drilling and core logging took place. Ten boxes of 'H' sized core, 61 mm (2.4 in.) in diameter, were taken from the mine site with a depth varying from 86 m to 118 m. This run of core included 22 m of channel sandstone. The sandstone channel was the particular material of interest, so this was the only material tested in the laboratory. Other overburden and underburden materials have been historically tested at this particular mine site and were not of specific interest for laboratory testing. The purpose of testing the channel sandstone was to determine accurate laboratory strengths and eventually rock mass strengths for input into the numerical models presented later. All laboratory testing was performed according to the ASTM standards D3967-08 (Brazil test) and D7012-10 (Unconfined compressive strength and elastic modulus).

4.1 Retrieval of Core (Channel Sandstone)

In summer 2011, two vertical core holes were drilled from the surface: BCX-2011-11C (11C) and BCX-2011-12C (12C). Continuous coring was performed from the surface to the termination depth of the boreholes. Core holes were bored with an 'H' sized, 3.05 m long, and single-tube core barrel. The core was logged for both holes, but

only collected for 12C. The purpose of 11C was for overburden logging and the determination of the fracture extent in the abutment zone. 12C was drilled from an elevation of 2,118 m to a depth of 118 m below the surface. Coal seam (D41 seam) thickness at this location was logged as 4.11 m with the sandstone channel in the roof of the coal separated by 0.49 m of fractured claystone and extending up 22 m.

The locations relative to the completed longwall panel are shown in Figure 4.1. Topography on the surface of the mine is relatively flat. From borehole 12C, core was retrieved for a depth ranging from 86 m (283 ft) to 118 m (387 ft) below the surface. This run of core included 22 m of channel sandstone material and 4.11 m of D41 coal. Precautions were taken such that each run of core was collected in sample bags to reduce moisture loss from the field to the laboratory. It is always good practice to maintain as much moisture in the samples so that the lab measurements accurately represent what is occurring in the field. Samples were taken to and prepared in the University of Utah rock mechanics laboratory.

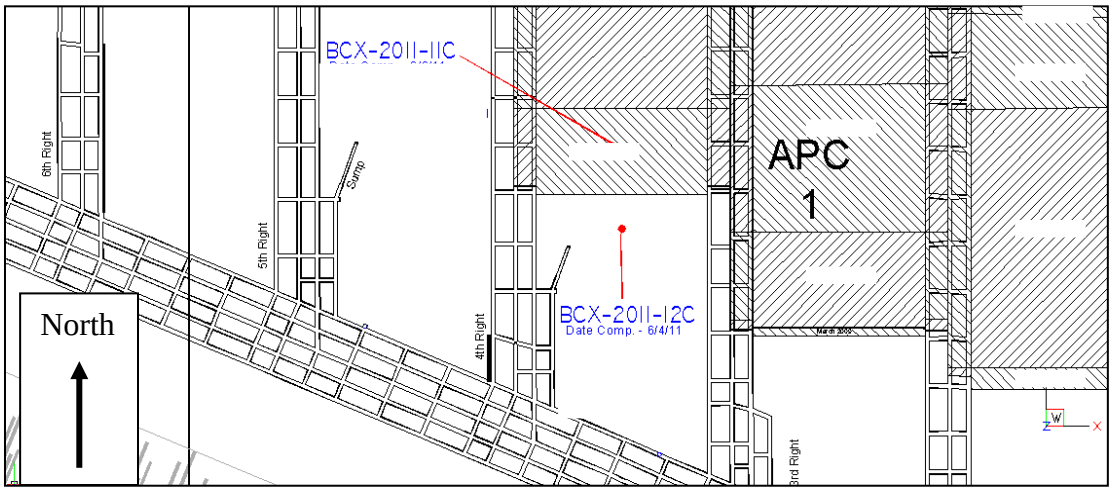

FIGURE 4.1 Locations of holes 11C and 12C relative to the completed longwall panel

4.2 Brazilian Test

Tensile strength of a rock may be determined by direct pull testing, bending, and indirectly by the popular Brazilian test. This test is also known as the "splitting" test (Pariseau 2006). A disk or cylinder of the material is loaded diametrically between the platens of a testing machine. Failure usually occurs by a splitting across the loaded diameter, and is valid only if the primary fracture initiates from the center of the specimen and spreads along the loaded diameter. The stress component normal to the loading diameter, σ_θ, and the stress component along the loading diameter, σ_r, are given by the following expressions (Vutukuri et al. 1974):

$$\sigma_\theta = +\frac{F}{\pi r_0 t\alpha}\left[\frac{\left(1-\left(\frac{r}{r_0}\right)^2\right)\sin(2\alpha)}{1-2\left(\frac{r}{r_0}\right)^2\cos(2\alpha)+\left(\frac{r}{r_0}\right)^4} - tan^{-1}\left(\frac{1+\left(\frac{r}{r_0}\right)^2}{1-\left(\frac{r}{r_0}\right)^2}\tan(\alpha)\right)\right] \tag{4.1}$$

$$\sigma_r = -\frac{F}{\pi r_0 t\alpha}\left[\frac{\left(1-\left(\frac{r}{r_0}\right)^2\right)\sin(2\alpha)}{1-2\left(\frac{r}{r_0}\right)^2\cos(2\alpha)+\left(\frac{r}{r_0}\right)^4} + tan^{-1}\left(\frac{1+\left(\frac{r}{r_0}\right)^2}{1-\left(\frac{r}{r_0}\right)^2}\tan(\alpha)\right)\right] \tag{4.2}$$

where, t is the thickness of the cylindrical specimen, r is the radius of the cylindrical specimen, and α is the angle across which force F is distributed (compression is negative). Thus, the value of σ_θ at the center of the cylinder can be an approximation of the tensile strength as follows:

$$\sigma_t = \frac{F}{\pi r_0 t}\left[\frac{\sin(2\alpha)}{\alpha} - 1\right] \approx \frac{F}{\pi r_0 t} \tag{4.3}$$

where, σ_t is the tensile strength and for simplicity, α approaches zero. This approximation of tensile strength assumes that failure is independent of stresses that develop normal to the disk face and thus is a plane-strain solution.

4.2.1 Laboratory Setup

Brazil disk samples were prepared in the laboratory such that the thicknesses of the disks were approximately 0.5 to 0.8 times the diameter. All of the samples were taken from core hole 12C for depths ranging from 91.4 m to 107.6 m and of the same channel sandstone material. Figure 4.2 shows the laboratory setup for the Brazilian test. The samples were placed between two platens and loaded with a hydraulic ram across the diameter until failure. Thirty two samples were tested in the laboratory using the Brazilian test. The results show that the average tensile strength of the channel sandstone is 0.523 MPa with a maximum and minimum of 1.012 MPa and 0.352 MPa, respectively. A summary of the results is shown in Table 4.1.

FIGURE 4.2 Laboratory setup and configuration for the Brazilian test

4.2.2 Results and Discussion

From the statistical analysis, a standard deviation of the sample set was found to be 0.135 MPa. This shows that the tensile strength of the channel sandstone does not have very much variation across the entire range of depths that it exists. Through a statistical analysis on the data set, one can be 95% confident that the mean lies between 0.474 MPa and 0.572 MPa. Thus, the results from the laboratory testing for tensile strength are satisfactory. Results and statistics for each sample can be found in the appendix of this paper.

4.3 Unconfined Compressive Strength and Young's Modulus

Unconfined compressive strength (UCS) is the most widely used property of rock for design. This strength parameter is widely used in the design of excavations because it represents the strength of a material that is not subject to confining stresses; this is often the case on excavation surfaces because they are free of normal and shear forces. From this, one can conclude that, regardless of depth of an excavation, the maximum compression that an excavation wall can withstand is the unconfined compressive strength (Pariseau 2006).

TABLE 4.1 Results of the Brazilian test

No. Samples	32
Average (MPa)	0.523
Maximum (MPa)	1.012
Minimum (MPa)	0.352
Std. Deviation (MPa)	0.135

Unconfined compressive strength test cylinders normally fail by fracture in the form of axial splitting, spalling or hour-glassing, single shear fracturing, or multiple fractures. Test cylinders are normally prepared so that the length of the specimen is approximately twice the diameter. The ends of the cylinders are then smoothed to promote as close to perfect parallelism as possible. Figure 4.3 shows a photograph of a prepared test cylinder of the channel sandstone tested in the University of Utah rock mechanics laboratory. The unconfined compressive strength of a rock material can be determined in the laboratory by applying an increasing axial load to the ends of a prepared rock cylinder until failure. The force applied at failure determines the unconfined compressive strength of the material based on the cross sectional area of the sample.

FIGURE 4.3 Photograph of a prepared cylinder of the channel sandstone material

The unconfined compressive strength can be calculated with the following:

$$UCS = \frac{P}{A} \tag{4.4}$$

where, P = failure load (N)

A = cross-sectional area of the cylinder (m^2)

UCS = unconfined compressive strength (Pa)

Young's modulus can also be determined from an unconfined compressive strength test if the displacement along the axis of the sample is measured during a uniaxial compression test. One can assume that if a rock material is loaded between two rigid platens and is in series with steel spacers, this system will act like stiff springs in series. Therefore, the stiffness method for determining Young's modulus is a viable approach. The formulation for calculating Young's modulus is as follows:

$$\frac{1}{K} = \frac{1}{K_S} + \frac{1}{K_r} \tag{4.5}$$

$$E = \frac{K_r L}{A} \tag{4.6}$$

where, K = total stiffness

K_S = stiffness of the steel

K_r = stiffness

E = Young's modulus

A = cross sectional area of the sample

L = length of the rock sample

Figure 4.4 shows a force (kN) vs. displacement (mm) plot for sample C8 and the spherical seat and spacer. The data in this plot show a failure load of 35.5 kN for the particular sample. The stiffness is shown in the plot as the slope of each line of 936.1 kN/mm and 78.52 kN/mm for the steel and total stiffness respectively. For the rock samples, the behavior is shown to be nonlinear near the beginning of the loading and near the end of the loading. Young's modulus is essential the elastic modulus of the material, so a linear best fit line was determined in the elastic range of the sample force-displacement curve to get the total stiffness K (kN/mm). K_s is the slope of the line produced by a separate test performed on the steel spherical seat and spacer.

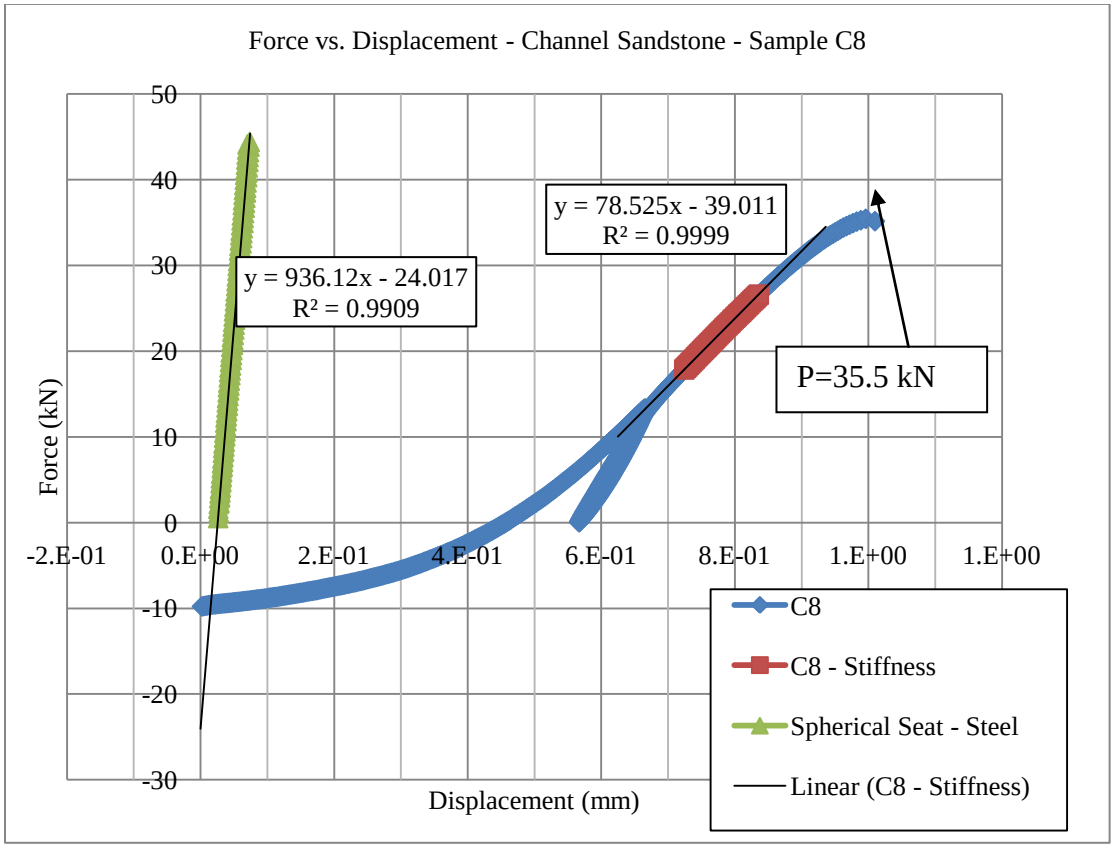

FIGURE 4.4 Force vs. displacement plot for channel sandstone sample C8

4.3.1 Laboratory Setup

Fourteen channel sandstone cylinders were prepared in the laboratory for unconfined compressive strength testing. Samples were approximately 61 mm (2.4 in.) in diameter and 127 mm (5 in.) in length. Preparations involved cutting the samples into ~127 mm segments and grinding the ends of each cylinder until end parallelism was reached. Each sample was then wrapped in plastic and put in sealed bags to ensure minimum moisture loss between preparation and testing. Samples ranged in depth from 91.1 m to 107.6 m. All of the samples were taken from core hole 12C. Figure 4.5 shows the laboratory setup for the compressive strength testing. Cylinders were loaded axially between two platens until failure.

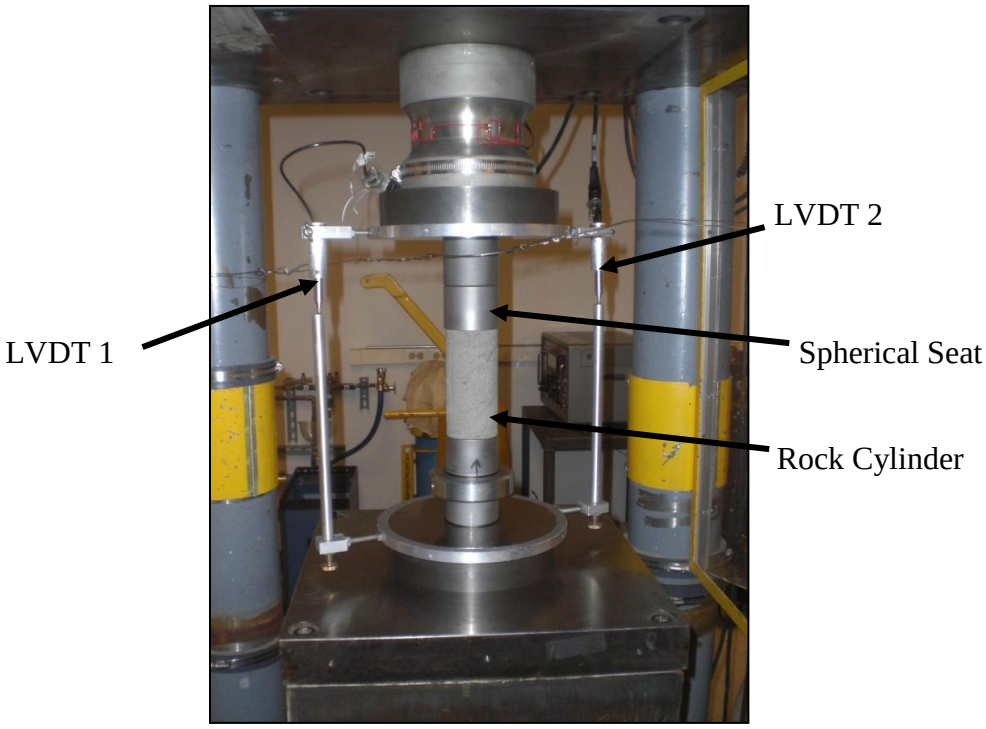

FIGURE 4.5 Laboratory apparatus used for the unconfined compressive strength tests.

Displacement measurements were determined from two linear variable differential transformers (LVDTs) oriented along the length of the sample. The average displacement value from the two LVDTs was used. High strength steel spacers and a spherical seat were also used as the interface between the platens and the rock sample. The spherical seat allows the compression along the length of the sample to be applied uniformly to the ends as the testing is performed. Force was measured with a hydraulic load cell attached to the testing apparatus. Data for each sample were collected by a computer and stored into a data file for analysis.

4.3.2 Results and Discussion

Fourteen samples were tested in the laboratory for unconfined compressive strength and Young's modulus. The results show that the unconfined compressive strength of the channel sandstone is 11.07 MPa with a maximum and minimum of 13.56 MPa and 7.66 MPa respectively. Results of the test summary, along with some statistics, are shown in Table 4.2. The standard deviation of the 14 samples testing for unconfined compressive strength is quite low. Through a statistical analysis on the data set, one can be 95% confident that the mean lies between 9.96 MPa and 12.17 MPa.

TABLE 4.2 Summary of UCS testing of channel sandstone

No. Samples	14
Average (MPa)	11.07
Maximum (MPa)	13.56
Minimum (MPa)	7.66
Std. Deviation (MPa)	1.908

From the 14 samples tested in the laboratory, the average Young's modulus of the channel sandstone is 3.63 GPa with a maximum and minimum of 4.46 GPa and 3.10 GPa, respectively. Through a statistical analysis on the data set for Young's modulus, one can be 95% confident that the mean lies between 3.35 GPa and 3.90 GPa. Table 4.3 summarizes the results of the Young's modulus testing. Tabulated results of all of the samples tested for unconfined compressive strength and Young's modulus can be found in the appendix section of this paper.

TABLE 4.3 Summary of Young's Modulus testing of channel sandstone

No. Samples	14
Average (GPa)	3.63
Maximum (GPa)	4.46
Minimum (GPa)	3.10
Std. Deviation (GPa)	0.469

5 COMPUTER SIMULATIONS

Numerical modeling of the umbrella pipe support system was performed in both two dimensions and three dimensions with the well known commercial software package FLAC. Finite difference grids were set up on a site specific basis to simulate the effect that a pipe umbrella would have on this particular western coal mine. Three models were constructed to simulate the following:

1. Pipe umbrella support over a single entry (FLAC 2D)
2. Pipe umbrella support over a single entry (FLAC 3D)
3. Directionally drilled pipe umbrella system over longwall recovery room (FLAC 3D)

The purpose of the numerical modeling was to derive a methodology for the design of pipe umbrella support in the underground coal mine setting. In the first and second models, the approach was to utilize the structural support elements within FLAC, specifically the beam elements, and embed them into the finite difference grid to simulate the umbrella pipes. The first model of System 1 is a two-dimensional plane-strain model, and the second model of System 1 is a three-dimensional model. The umbrella pipes undergo loading due to undermining and bending moments develop due to the deformation of the grid. This bending moment varies based on the mechanical properties of the beam element and also the spacing of the beams over the mine entry. Thus, one can perform a safety factor analysis of each variation of pipe diameter and spacing based on

the previously explained analytical method for pipe umbrella support. Three pipe geometries were analyzed in Models 1 and 2: 114 mm, 139 mm, and 168 mm diameters.

In the third model, the approach was to model the effect that a reinforced zone comprised of a double layered pipe mesh of 114 mm diameter pipes filled with grout had on the stresses and displacements over a longwall recovery room. Instead of explicitly modeling beam elements, a composite reinforced zone was inserted into the model above the longwall recovery room on the headgate side. In addition to modeling the mesh reinforcement benefits, the third model was used to capture the overall response of the strata mechanics due to longwall mining and compare the subsidence profile of the model to actual subsidence measurements at the mine. The abutment stress distribution relative to the longwall face was also captured and compared to established empirical formulae as a validation exercise.

5.1.1 Numerical Modeling in Geomechanics

In science and engineering, accuracy is the degree to which a measurement or calculated quantity matches its true value. Precision is closely related to accuracy, but different in concept. Precision is the degree to which repeated measurements or calculations consistently produce the same or similar results (Hammah et al. 2009). Modeling in the geomechanics field has the ubiquitous presence of large uncertainty and one can produce erroneous results without a good technical base of the subject matter. Generally speaking, bad input parameters lead to bad outputs in a numerical model. It is better to use approximate inputs and yield an approximate result, rather than using precise inputs and yielding a precise output; this precise output could be exactly wrong.

Models, in general, serve as important tools in science and engineering and help its users to predict and understand phenomena that cannot be measured easily in the field. In the field of geomechanics, models are used as tools to aid mine operators, contractors, and consultants in making better design decisions. A model can then be defined as a representation of a system that allows us to investigate the behavior and attributes of a system, and sometimes, predict the outcomes of the system under various conditions. This is particularly helpful when parametric studies are performed or an uncertainty of inputs is evident.

5.1.2 Finite Difference Method (FDM) in FLAC

Finite difference analysis in FLAC is a complex and rigorous way for solving boundary value problems, such stress and strain in a continuum and at an excavation boundary due to undermining. In stress analysis, equations of equilibrium, strain-displacement relationships, and stress-strain laws are met under the constraints specified at the boundaries of the region of interest. FLAC implements approximate solutions to differential equations by replacing derivative expressions with approximately equivalent difference quotients. The difference quotients are defined by the geometry of grid points and zones in FLAC.

The physical processes in FLAC are time-dependent and obtain solutions to approximate differential equations in an *explicit* method, i.e., the state of the system is calculated at a later time from the current. The central concept is that the calculation "wave speed" always keeps ahead of the physical wave speed, so that the equations always operate on known values that are fixed for the duration of the calculation. The

incremental displacements from each time step are added to the coordinates so that the grid moves and deforms with the material it represents; this is termed a "Lagrangian" formulation. Grid values are updated after each time step. The FDM is a good method for problems that expect large deformations from the original geometry. Figure 5.1 shows a general layout of a finite difference grid, where nodes are expressed in terms of *i* and *j*. Geometric locations of the nodes are expressed as *x* and *y*.

The behavior of the numerical model is computed based on the dynamic equations of motion coupled with some constitutive law for stress and strain. Velocities and displacements are computed at each grid point. Stress and strain are functions of the force applied on area.

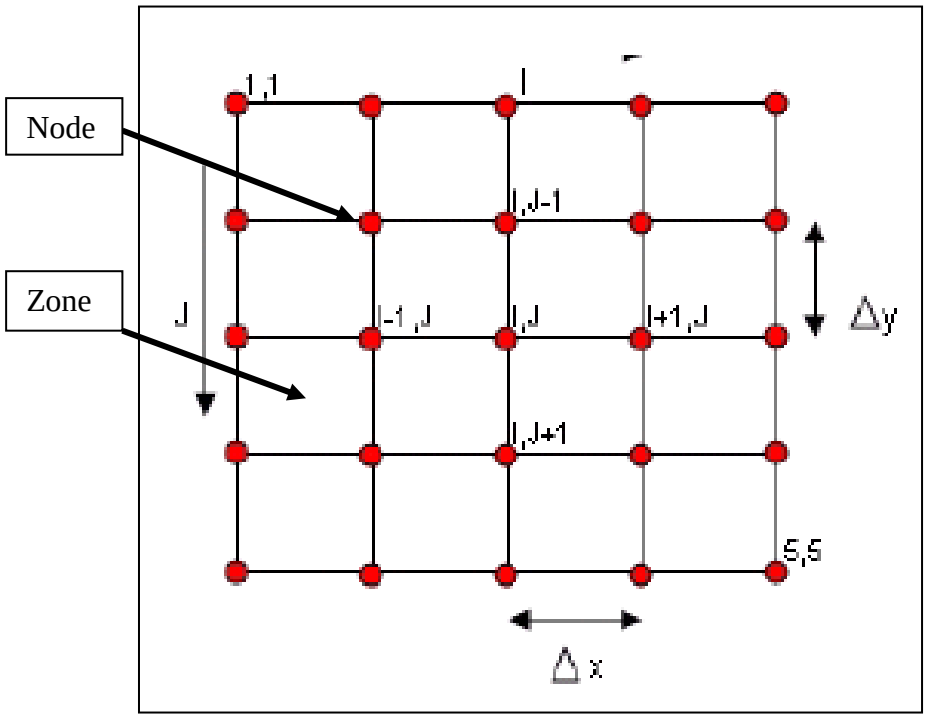

FIGURE 5.1 General layout of a finite difference mesh showing nodes and zones

Therefore, the stresses and strains are calculated for each zone and assigned to the centroid of a zone where a force is acting. In a continuous solid body, the general dynamic equation can be generalized as follows (Itasca 2005):

$$\rho \frac{\delta \dot{u}_i}{\delta t} = \frac{\delta \sigma_{i,j}}{\delta x_i} + \rho g_i \tag{5.1}$$

where, ρ = mass density

t = time

x_i = components of coordinate vector

g_i = components of gravitational acceleration (body forces)

$\sigma_{i,j}$ = components of stress tensor

For stress analysis, the differential equations for a solid, one-dimensional bar can be expressed in terms of a constitiutive law (Hooke's Law):

$$\sigma_{xx} = E \frac{\delta u_x}{\delta x} \tag{5.2}$$

and the law of motion (or equilibrium):

$$\rho \frac{\delta^2 u_x}{\delta t^2} = \frac{\delta \sigma_{xx}}{\delta x} \tag{5.3}$$

The numbering scheme for zones and grid points in the one-dimensional problem as used in FLAC is shown in Figure 5.2. Zones and nodes are labeled in separate numbering schemes to conserve consistency and keep velocities and displacements separate from stresses.

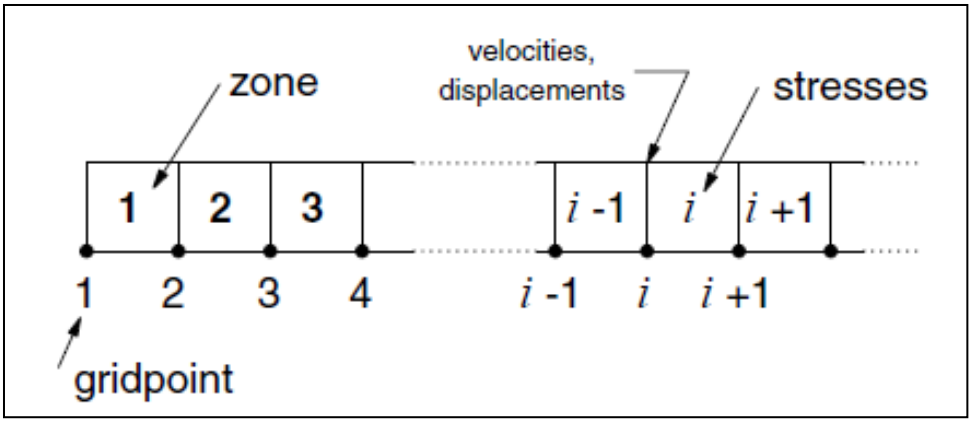

FIGURE 5.2 Numbering scheme for zones and grid points in FLAC

The finite difference approximations for equations 5.4 and 5.5 can be written as follows:

$$\sigma_{xx}^{i}(t) = E\frac{u_x^{i+1}(t) - u_x^{i}(t)}{\Delta x} \tag{5.4}$$

$$u_x^{i}(t + \Delta t) = u_x^{i}(t) + \dot{u}_x^{i}\left(t + \frac{\Delta t}{2}\right)\Delta t \tag{5.5}$$

where, σ_{xx} = stress in the x direction

E = elastic modulus

u_x = displacement in x direction

$\dot{u}_x$ = velocity in the x direction

t = time

x = location along the x-axis

In this formulation, the equation of motion has been integrated twice so that displacements are explicitly calculated. The quantities on the right-hand sides of the

difference equations are known, so equation 5.5 must be evaluated first for all zones before the equation of motion can be used. In concept, this calculation concept of time stepping is the same as a simultaneous update of variables (Itasca 2005). Figure 5.3 shows the calculation steps that FLAC implements for each time step.

5.1.3 Beam Elements in FLAC

Beam elements in FLAC are standard two-dimensional or three-dimensional elements with 3 degrees of freedom in FLAC2D and 6 degrees of freedom in FLAC3D (rotation and translation) at each node. Typically, the beam elements are considered to behave as a linear elastic material and are defined by material and geometric properties, i.e., modulus, area, and second moment of inertia (Itasca 2005). Figure 5.4 shows a depiction of a structural element as utilized in FLAC.

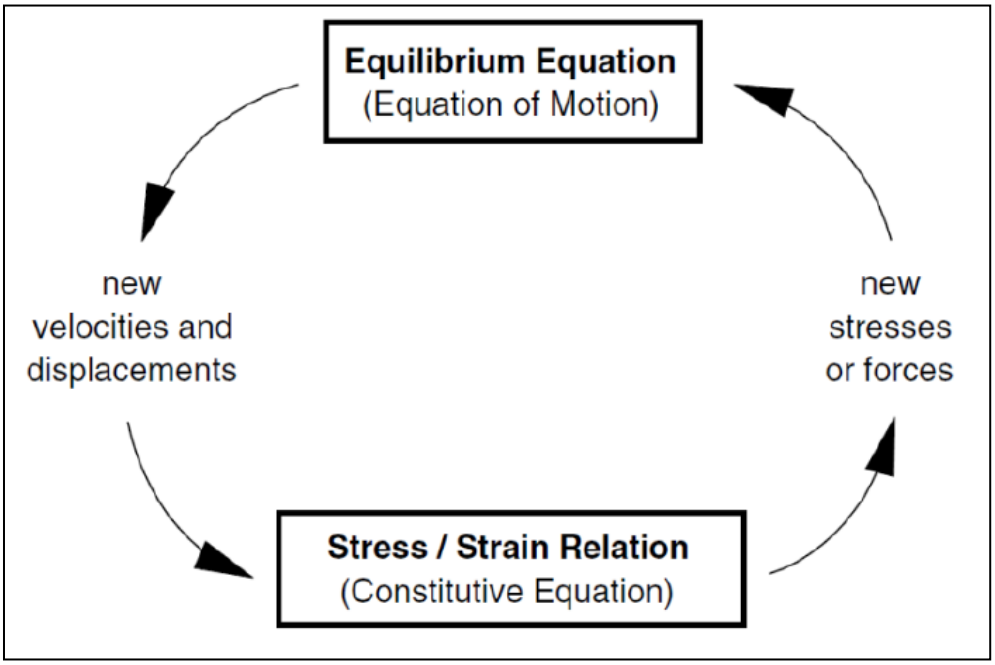

FIGURE 5.3 Time marching calculation steps in FLAC

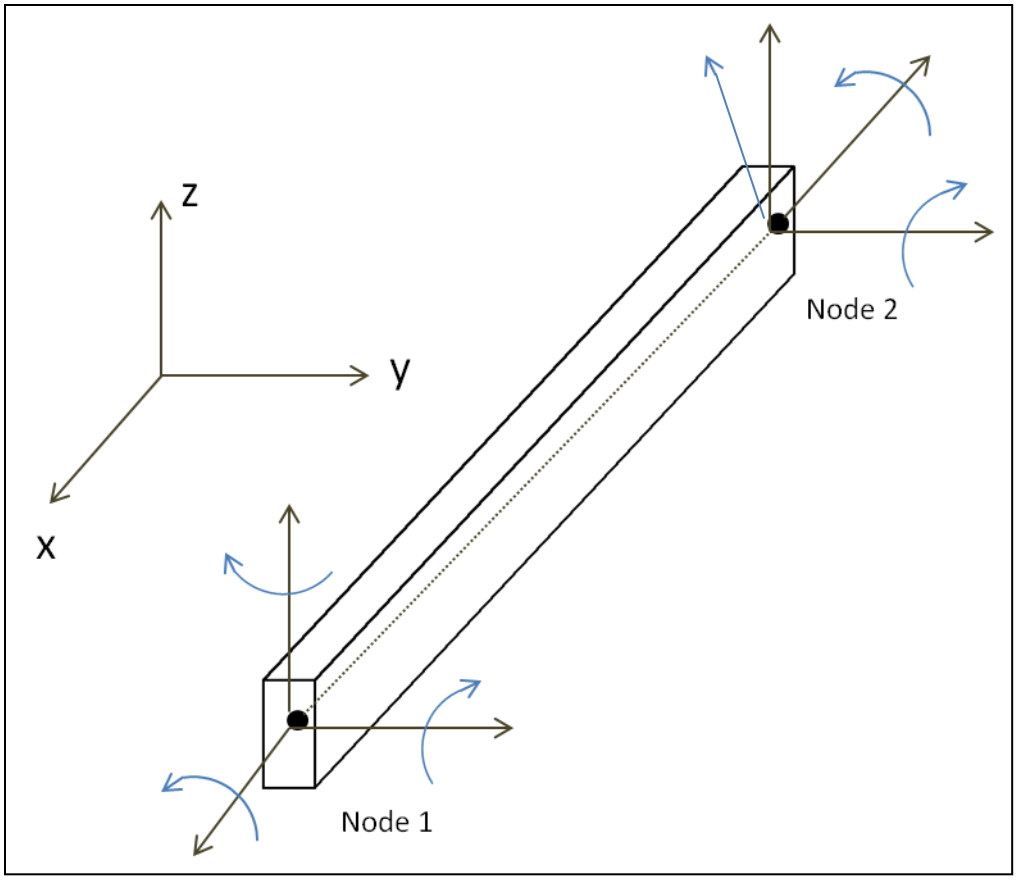

FIGURE 5.4 Beam element as employed in FLAC

In two dimensions, the beam elements are modeled in a plane-stress formulation. If spaced reinforcement is to be simulated, such as a pipe umbrella system in two-dimensions, the spacing in the out-of-plane direction can be specified within the FLAC model. The spacing parameter, entered in units of length, is used to automatically scale the properties and parameters of the beam element to account for the effect of the distribution of the beams over a regularly spaced pattern. In three-dimensions a spacing parameter is not required, and the beam is allowed to rotate along its axis as well as translate in all dimensions.

5.1.4 FLAC Model Stratigraphic Column

Based on the core logging information for core hole BCX-2011-12C, a generalized statigraphic column was constructed for use in numerical modeling. The thickness and material type for each layer is shown below in Figure 5.5. Generally, it is not numerically economical to model each rock layer in a stratigraphic column. Combining varying stratified deposits into larger units is good practice, as it is much simpler to manage in a numerical model and the results are generally the same as a more complex model.

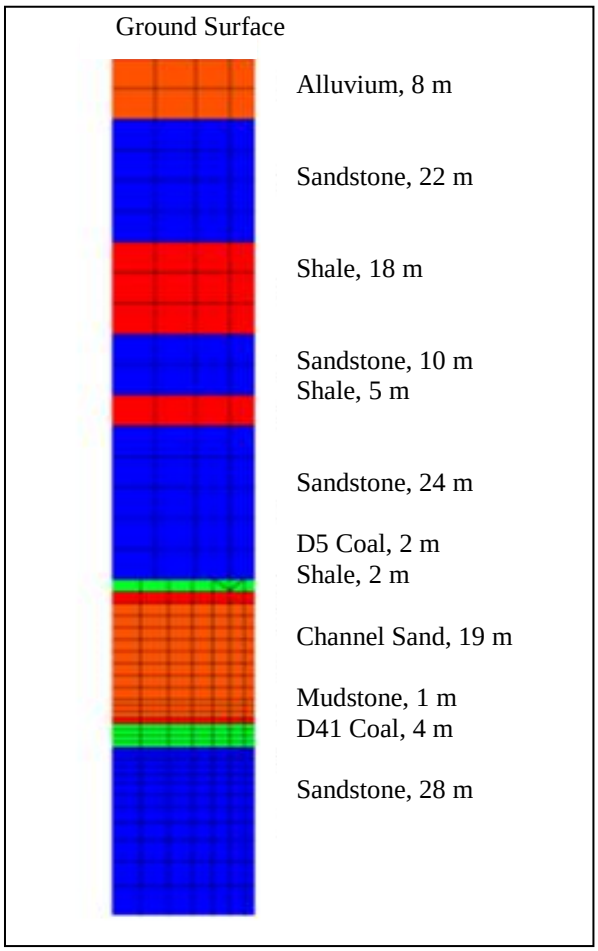

FIGURE 5.5 Generalized stratigraphic column for input into FLAC models

5.1.5 Material Properties

A suite of material properties was adopted for the numerical model based on recent laboratory testing performed in this study and historical data provided by the mine. Most importantly, the channel sandstone was analyzed in the laboratory and adjusted to the field scale using the Rocscience software Roclab. Overburden and underburden material properties were also scaled from lab strengths to rock mass strengths. Roclab uses the previously explained methodology for determining equivalent Mohr-Coulomb parameters from the Hoek-Brown rock mass strength criterion. The following material properties, as shown in Table 5.1, were assumed for the analysis. For the highly weathered rock, as in the strata of the western U.S. coal mine, a GSI of 45 was assumed for all layers.

All material, except for the gob and any reinforced zones, were considered to follow the Mohr-Coulomb constitutive relationship in the FLAC code. The Mohr-Coulomb model assumes elastic behavior until a failure point is reached, then the material behaves perfectly plastic. Inputs into the FLAC model include density, bulk modulus, shear modulus, cohesion, and friction angle.

TABLE 5.1 Material properties used in FLAC modeling

Formation	ρ (kg/m^3)	c (MPa)	phi (deg)	UCS (MPa)	T_0 (MPa)	E (MPa)	v	K (MPa)	G (MPa)
Coal	1,329	1.028	34	3.76	0.422	1,638	0.35	1,820	607
Shale	2,354	0.543	21	0.32	0.016	264	0.24	169	106
Sandstone	2,450	1.249	35	1.29	0.029	2,160	0.39	3,273	777
Channel Sand	2,370	0.606	34	0.37	0.005	579	0.27	419	228
Alluvium	1,750	0.002	28	-	-	9.00	0.49	300	100
Gob	1,750	-	-	-	-	Varies	0.30	Varies	Varies

5.2 Analytical Calculations for System 1 Pipe Umbrella

The system of a pipe umbrella system over a single coal mine entry is very similar to the configuration of a statically indeterminate beam with two fixed ends and a uniformly distributed load. The geometry of the pipe umbrella system as used in the analysis is shown in Figure 5.6. The assumption is that a single pipe can be analyzed as a beam in bending and that the loading on the pipe varies based on the spacing of the pipes across the horizon. The zone encompassed by the red dotted line is assumed to fail. Therefore the weight of the rock above the umbrella pipes in the yield zone must be completely supported. Varying the pipe spacing and yield height will change the volume of rock that applies its dead weight on the beam. Fixed ends are assumed as the boundary conditions of the system because of the fact that the pipe umbrella system is embedded in the rock and grouted in place, therefore the rotation of the beams ends is not allowed i.e. the highest moment exists at the beam ends.

The height of the yield zone of approximately 3.5 m to 5.5 m was determined using the empirical methodology proposed by Terzaghi (1946) for estimating height of yield zone in a single tunnel configuration in "Very blocky and seamy" rock, where:

$$H_P = (0.35\ to\ 1.10)\ (B + H) \tag{5.6}$$

where, H_P = height of yield zone, m

B = width of entry, m

H = height of entry, m

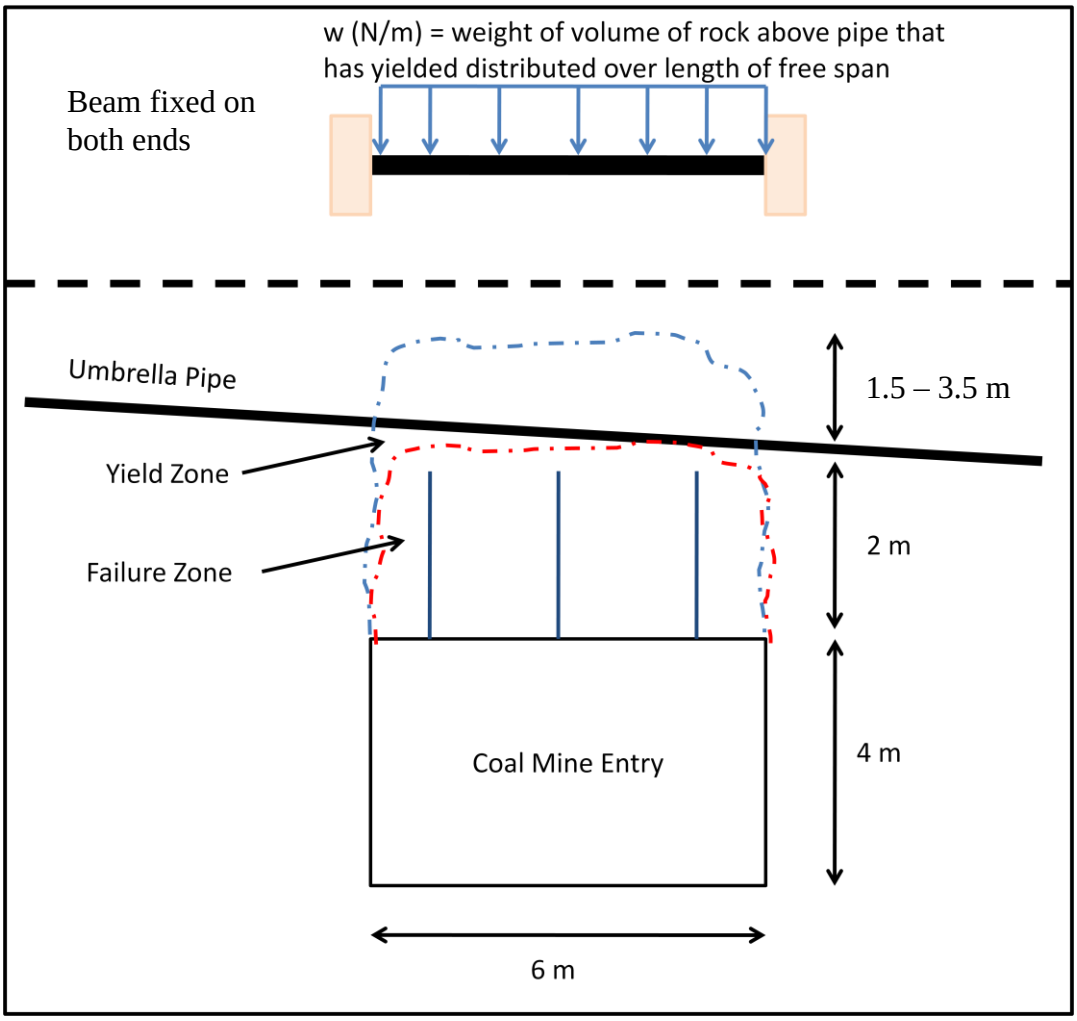

FIGURE 5.6 Geometry of a pipe umbrella system over a single entry

If a free body diagram is constructed of a beam with two fixed ends, one will find that the beam is indeterminate to the first degree, where *M'* is redundant. *M'* is the reactive moment at the ends of the beam, and is the maximum moment that the beam experiences. Figure 5.7 is a depiction of the free body diagram for a beam with two fixed ends and an evenly distributed load. In the analysis of the pipe umbrella system over a single entry, the free span of the beam (*L*) is considered to be 6 m.

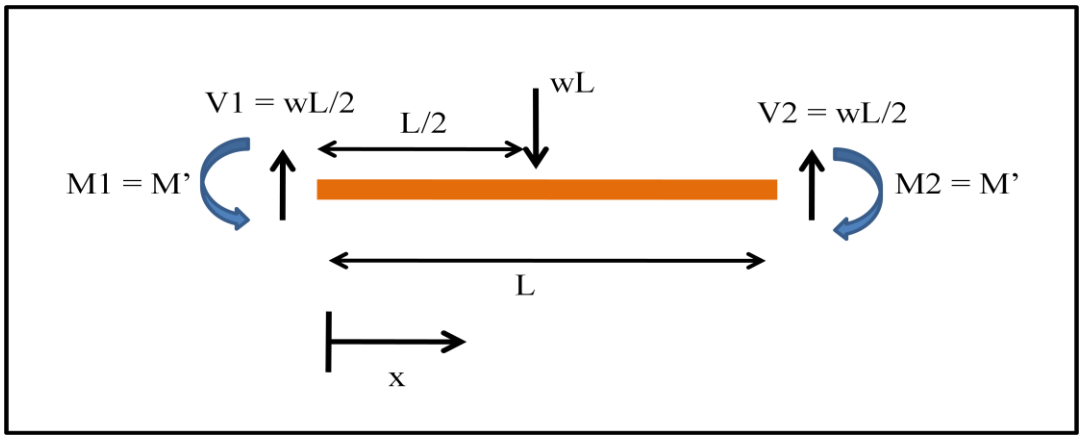

FIGURE 5.7 Free body diagram of a uniformly distributed beam with fixed ends

From the free body diagram, the internal moment, *M*, can be expressed in terms of *M'* as follows (Hibbeler 2005):

$$M(x) = \frac{wL}{2}x - \frac{w}{2}x^2 - M' \tag{5.7}$$

where *M(x)* is the internal moment of the beam at a distance *x*, *w* is the magnitude of the distributed load (force), *L* is the free span of the beam, and *M'* is the internal moment of the beam at the fixed ends.

Assuming,

$$EI\frac{d^2v}{dx^2} = M(x) \tag{5.8}$$

and after a double integration of equation 5.8, it becomes

$$EIv = \frac{wL}{12}x^3 - \frac{w}{24}x^4 - M'x^2 + C_1x + C_2 \tag{5.9}$$

where v is the deflection of the elastic curve of the beam, E is the elastic modulus of the beam material, I is the area moment of inertia of the beam, and C_1/C_2 are constants of integration defined by the boundary conditions of the system.

With the aid of boundary conditions ($v=0$ *at* $x=0$, $\frac{dv}{dx} = 0$ *at* $x=0$, *and* $v=0$ *at* $x=L$), M', C_1, and C_2 can be determined. Assuming the given boundary conditions, C_1 and C_2 are equal to *0*. This yields the following equation for the maximum moment experienced by a beam with fixed ends and a uniformly distributed load:

$$M' = \frac{wL^2}{12} \tag{5.10}$$

This method of solution for finding the maximum moment in the statically indeterminate beam is generally suitable when only one x coordinate is required to describe the elastic curve of the beam. Note that if more than one x-coordinate is needed (location of maximum moment), and then the equation of continuity must be written, complicating the calculation process (Hibbeler 2005).

For the analysis of the current problem, the weight of rock resting on the pipes can be calculated by the unit weight of the yielded sandstone material, the spacing of the pipes, and the free span of the beam. The unit weight of the sandstone material (γ) was measured to be 23.25 kN/m^3. The spacing of the pipes was varied from 0.25 m to 2.0 m, therefore giving a wide range to be analyzed for each pipe. The distributed load (w) for the pipe umbrella geometry depicted in this paper is calculated by the following:

$$w = \frac{BHS\gamma}{L} \text{ (kN/m)} \tag{5.11}$$

where B = entry width, m

H = height of failure zone above the umbrella pipe, m

S = spacing between umbrella pipes, m

γ = unit weight of roof material, kN/m^3

L = length of free span of the pipe (entry width), m

5.2.1 Design

Design of proper spacing between pipes of a pipe umbrella system above a coal mine entry can be performed based on the bending stress that a single pipe in the series experiences. The max bending stress in the beam can be calculated using the flexure formula. Using the assumption of a beam in bending the flexure formula is as follows (Hibbeler 2005):

$$\sigma_B = \frac{M'c}{I} \tag{5.12}$$

where I = area moment of inertia for the pipe beam

c = distance from the center of the pipe to the outer most fiber

M' = maximum moment experienced in the beam from equation 5.12

The area moment of inertia *(I)* is calculated for a tube beam geometry using the following formula (Hibbeler 2005):

$$I = \frac{\pi}{64}(D_0^4 - D_i^4) \tag{5.13}$$

Therefore, the safety factor of the beam in bending can be calculated as follows:

$$FS = \frac{\sigma_Y}{\sigma_B} \tag{5.14}$$

where, σ_B = maximum bending stress of the beam

σ_Y = yield strength of the steel in the pipe

5.2.2 Results

Employing the above analytical methodology for calculating the safety factor of various pipe spacing configurations, a plot was constructed showing the safety factor of the pipe umbrella support system over a single entry. Table 5.2 shows the assumed properties of the beam used in this analysis. Figure 5.8 shows the safety factor vs. the spacing for three types of casing: 114 mm, 139 mm, and 168 mm, respectively. Note that this plot is showing the results for a yield height of 1 m above the pipe umbrella. Thus, each pipe is supporting the weight of a 1 m x 6 m x spacing (m) block of rock. Further in this paper, the results of the analytical calculation for 2 m and 3 m yield height above the pipe umbrella are presented in comparison to numerical models of the same geometry.

TABLE 5.2 Yield strength, elastic modulus, and area moment of inertia for umbrella pipes

Beam Type	Yield Strength (MPa)	Elastic Modulus (GPa)	Area Moment of Inertia, I (m^4)
114 mm	700	215	$3.127\ (10)^{-6}$
139 mm	700	215	$7.203\ (10)^{-6}$
168 mm	700	215	$1.858\ (10)^{-5}$

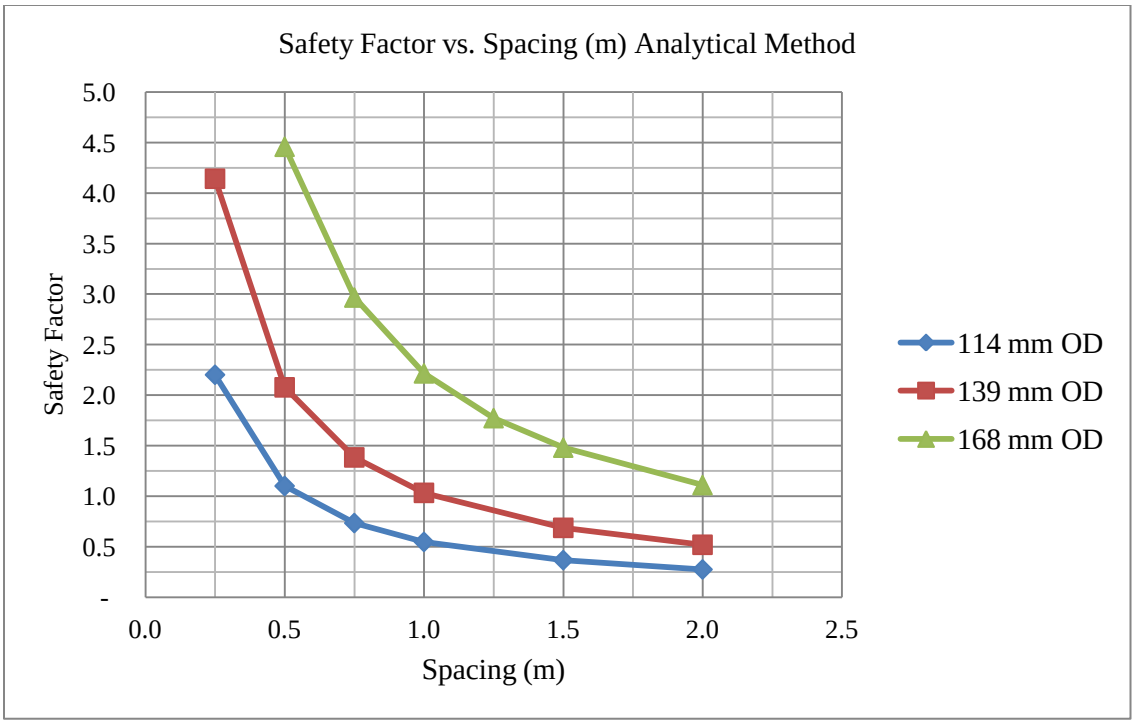

FIGURE 5.8 Safety factor vs. Spacing plot for analytical calculations of 1 m yield height

5.2.3 Discussion

A safety factor less than 1 indicates that the pipes subject to a bending stress are past their elastic limit. Pariseau (2006) recommends that a safety factor of 1.5 be applied for steel structural supports in tunneling. Using design criteria for a safety factor of 1.5, the required spacing for the various pipes is 0.4 m, 0.75 m, and 1.5 m for 114 mm, 139 mm, and 168 mm casing, respectively.

The safety factor calculation shows what spacing of pipes is needed for the various diameters. Each configuration would perform its respective duty, however, the designer must take into account the feasibility of drilling a 114 mm borehole vs. a 168 mm borehole; of course it would be much easier to drill a 114 mm borehole and install the casing, but the spacing would be much closer and problems may arise with borehole

deviation and the intersection of parallel holes. The deviation of a borehole path can be controlled by accurate drilling and surveying methods.

In this crude calculation, the material that might break up and fall between the pipes was not taken into account. The point of a supplementary support system, such as a pipe umbrella system, employed in a coal mine setting is to prevent additional material from failing above a current roof bolt system. If this is the case, then one might choose to design the pipe umbrella system with a closer spacing. Larger pipe diameter may be desired if the yielded material above the entry is massive, so that the spacing between pipes can be increased. This will result in less drilling footage. There is always the tradeoff between more footage of a smaller diameter vs. less footage of a larger diameter. The designer of this type of system must take into account not only the loads that a pipe undergoes, but also the overall quality of rock, e.g., RQD, RMR, GSI, etc. If the rock mass has small joint or fracture spacing in various orientations, then it is more prone to fail between pipes of larger spacing.

In the case presented in this study, the material in the roof is massive, with an RQD greater than 95%. This means that the material is very blocky and will more than likely not fail between the pipes if it is pre-supported. In the current study, the recommended pipe configuration is the 139 mm casing at a spacing of approximately 0.75 m based on the analytical calculations.

5.3 System 1: Pipe Umbrella Over Single Entry - FLAC 2D

The first model of System 1 is a two-dimensional plane-strain simulation of a cross section taken through a typical three entry gate-road section at the western U.S. coal mine. The model extends from the top of the D5 coal seam, down to 25 m below the

mined D41 coal seam. Overall dimensions of the finite difference grid are 110 m and 56 m for width and height respectively. Entries excavated in the coal seam are 6 m by 4 m and pillars are of varying widths of 25 m and 18 m. These dimensions are consistent with actual dimensions at the mine.

5.3.1 FLAC 2D Model Boundary Conditions

Displacements normal to the sides and bottom of the mesh shown in Figure 5.9 are not allowed, that is, they are fixed at zero. A constant stress equal to the overburden stress above the D5 coal seam was applied to the top of the model. For an average specific weight of 23 kN/m^3, this constant stress applied to the top boundary is 2 MPa for a depth of overburden of 87 m to the D5 coal seam. Displacements are not fixed on this boundary, so the top is essentially a free surface and is allowed to move as excavation dictates; however, it is confined by the applied vertical stress. Figure 5.9 shows the overall geometry of the FLAC 2D model.

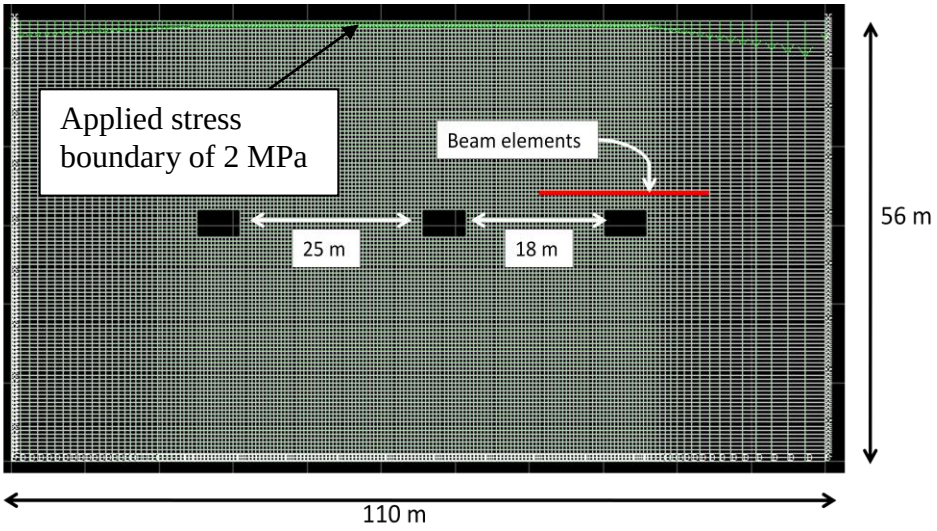

FIGURE 5.9 Cross-section of System 1 model in FLAC 2D

5.3.2 FLAC 2D Model Initial Conditions

Initial conditions for stress were determined based on gravity loading for the vertical stress and a combination of the vertical stress and a tectonic stress for the horizontal stress. The average weight of the overburden was calculated to be 23 kN/m^3, so the vertical stresses at the top and bottom boundaries were 2 MPa and 3.2 MPa, respectively (linear variation between). The horizontal principal stress were calculated based on the method proposed by Esterhuizen et al. (2009), where the major and minor principal horizontal stresses vary based on the vertical stress component and the elastic modulus of the material. Plane strain conditions imply that there is an out-of-plane horizontal stress, thus both major and minor principal stresses in the horizontal directions were used as model inputs. A stress transformation step was also performed because the horizontal principal stresses at the mine are oriented N 40° W and the headgate entries are oriented due north.

5.3.3 FLAC 2D Modeling Steps

After the initialization of the in-situ stresses, a single excavation step was performed to simulate mining of the headgate entries. The purpose of the FLAC 2D model was to analyze the behavior of a pipe umbrella system during the development portion of the longwall retreat mining process. Additional stresses that developed in the mesh were only due to the excavation of the three entries.

Simulations were carried out in essentially three steps. The first step was the initial set-up of the grid, material properties, boundary conditions, and initialization of the in-situ stress data. The model was then solved to equilibrium. Secondly, the beam

elements were tied to each node (0.5 m in length each) and to each other to represent a single beam at a distance of 2 m above the excavated entry. The entries were then excavated and the model was cycled until the displacements (roof sag) stopped changing. A yield zone in the roof developed. The extent of the yield zone is approximately 2 m, as shown in Figure 5.10. Brown indicates that the zone is above the elastic limit, red means the zone is in volumetric or shear strain yield, yellow indicates failure in tension, and pink means that the material is still in the elastic range. As the final step in the modeling process, the yield zone depicted in Figure 5.10 was excavated (nulled) from the FLAC grid. This simulated the complete failure of the roof bolts.

The process was repeated six times for each pipe dimension at out-of-plane beam spacing varying between 0.25 m and 2.0 m. The parameters that change in each iteration of the FLAC 2D model are the spacing between beam elements and the geometric dimensions of the beam elements.

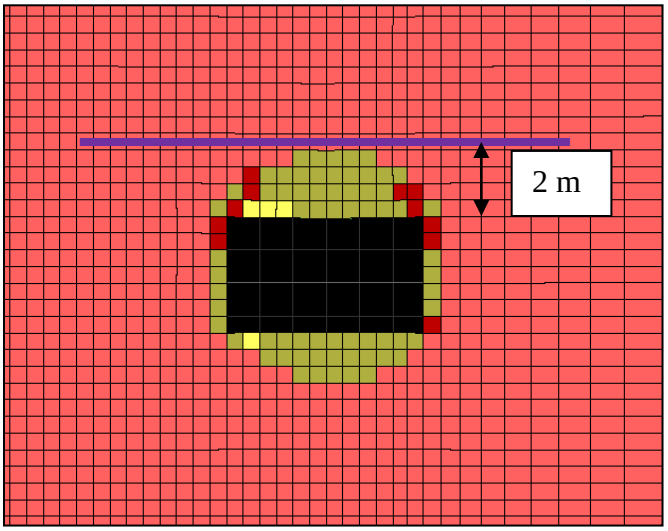

FIGURE 5.10 Extent of yield zone above a single entry from FLAC 2D

Eighteen variations of the FLAC 2D model were run. The important output from each model is the maximum bending moment that any of the beam elements experienced. From the bending moment, one can calculate the maximum normal stress in the beam due to bending and a safety factor based on the yield strength of the steel in the pipe.

5.4 System 1: Pipe Umbrella Over Single Entry - FLAC 3D

The second model of System 1 is a simple three-dimensional analysis of a single entry 4 m by 6 m excavated with beam elements installed in the grid as a simulation of a pipe umbrella system. This model is similar to the FLAC 2D model, but only a single entry was modeled due to the symmetrical conditions of a three entry gateroad section during development. The parallel entries, as in the first model, did not have any significant impact on the stress and displacements on the analyzed entry. Thus, a single entry was modeled to decrease the computational time for each model. A total of 184,000 zones were employed in the FLAC 3D model and they were discretized to a 0.5 m by 0.5 m resolution near excavation boundary. The overall geometry of the FLAC 3D model for System 1 is depicted in Figure 5.11.

5.4.1 FLAC 3D Model Boundary Conditions

Displacements normal to the sides and bottom of the mesh shown in Figure 5.12 are not allowed, that is, they are fixed at zero. For an average specific weight of 23 kN/m^3, this constant stress applied to the top boundary is 2 MPa for a depth of overburden of 87 m to the D5 coal seam. The top surface is free to move as excavation dictates, although it is confined by the applied 2 MPa stress boundary.

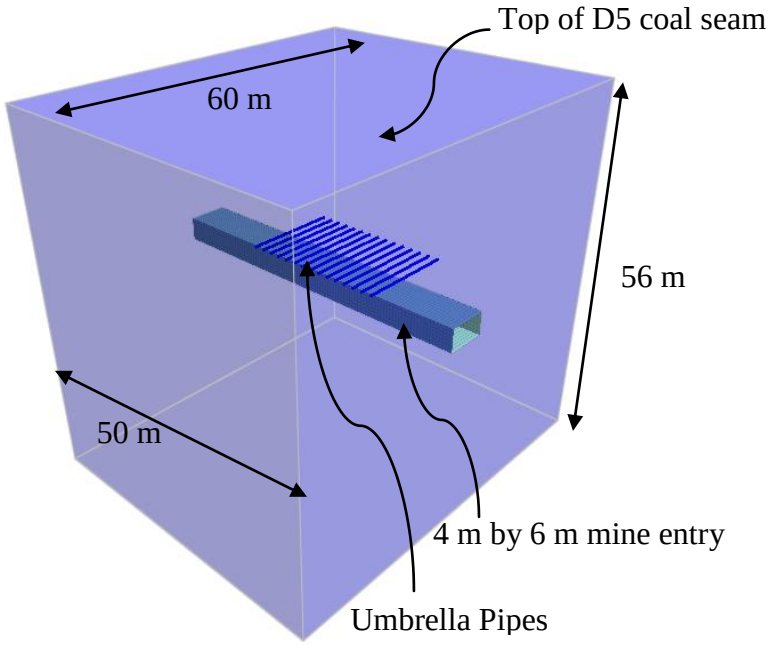

FIGURE 5.11 Overall geometry for the FLAC 3D model of System 1

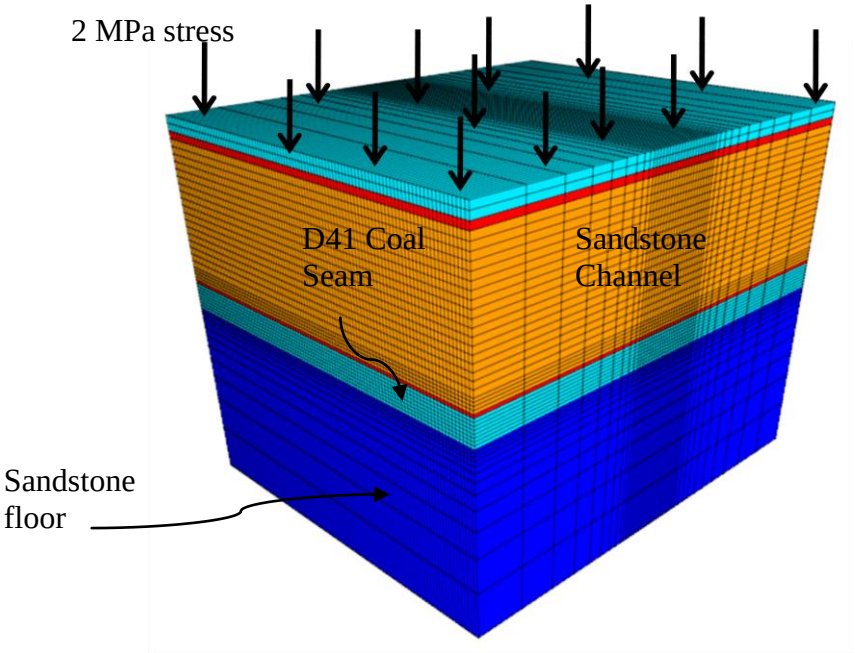

FIGURE 5.12 Geometry of FLAC 3D model of System 1 showing the material layers

5.4.2 FLAC 3D Model Initial Conditions

Much like the FLAC 2D model, the initial conditions for stress were determined based on gravity loading for the vertical stress and a combination of the vertical stress and a tectonic stress for the horizontal stress. The average weight of the overburden was assumed to be 23 kN/m^3, so the vertical stresses at the top and bottom boundaries were 2 MPa and 3.2 MPa respectively (linear variation between). The horizontal principal stress were calculated based on the method proposed by Esterhuizen et al. (2009), where the major and minor principal horizontal stresses are suggested to vary based on the vertical stress component and the elastic modulus of the material.

Since this is a fully three-dimensional model, both major and minor principal stresses in the horizontal directions were used as model inputs. Stress transformation was also performed due to the fact that the horizontal stresses at the western U.S. mine were determined to be N 40° W and the development entries are oriented due north.

5.4.3 FLAC 3D Modeling Steps

First, a single excavation step was performed to simulate mining of the single entry. The purpose of the FLAC 3D model was to analyze the behavior of a pipe umbrella system during the development portion of the longwall retreat mining process. Additional stresses that developed in the mesh were only due to the excavation of the single entry.

Simulation of the model was carried out in three steps. The first step was the initial set-up of the grid, material properties, boundary conditions, and initialization of the in-situ stress data. The model was then solved to equilibrium. Next, the beam elements

were inserted in to the model and tied to each zone (1.0 m in length each) and to each other to represent a single beam at a distance of 2 m above the excavated entry. Unlike FLAC 2D, the beam elements each have six degrees of freedom and spacing between each beam does not need to be entered as a single parameter. Rather, the actual locations of each element are specified during the model building process. The entries were then excavated and the model was cycled until the displacements (roof sag) stopped changing. Similar to the FLAC 2D model, a yield zone in the roof developed. As the final step in the modeling process, the yield zone was excavated (nulled) from the FLAC grid. This simulated the complete failure of the roof bolts.

5.5 Results of System 1 Modeling

The results of the modeling exercises performed for System 1 are presented in this section. For each model run, a maximum bending stress was calculated based on the maximum moment output. Similar to the analytical calculation of System 1, the maximum moment was used to calculate a bending stress and a safety factor for each condition of spacing and pipe geometry. Table 5.3 shows the results for the modeling performed in FLAC 2D.

The data in Table 5.3 show that a safety factor of at least 1.5 can be achieved if a regular spacing between pipes is between 0.25 m and 1.0 m. This, of course, will depend on the geometry and strength of the pipes selected for use. In this analysis, high strength steel with yield strength of 700 MPa was assumed. For the results presented, the spacing required for a safe design are 0.375 m, 0.5 m, and 1 m for 114 mm, 139 mm, and 168 mm diameter casing, respectively. Figure 5.13 depicts these results graphically.

TABLE 5.3 Bending stress and safety factors for System 1 modeling in FLAC 2D

Spacing (m)	Bending Stress FLAC 2D (MPa)			Safety Factor FLAC 2D		
	114 mm	139 mm	168 mm	114 mm	139 mm	168 mm
0.25	385.25	328.12	279.45	1.82	2.13	2.50
0.50	597.79	518.59	361.21	1.17	1.35	1.94
0.75	752.77	679.70	436.45	0.93	1.03	1.60
1.00	875.58	816.66	510.97	0.80	0.86	1.37
1.50	1,054.68	1,058.39	570.66	0.66	0.66	1.23
2.00	1,174.93	1,211.61	686.88	0.60	0.58	1.02

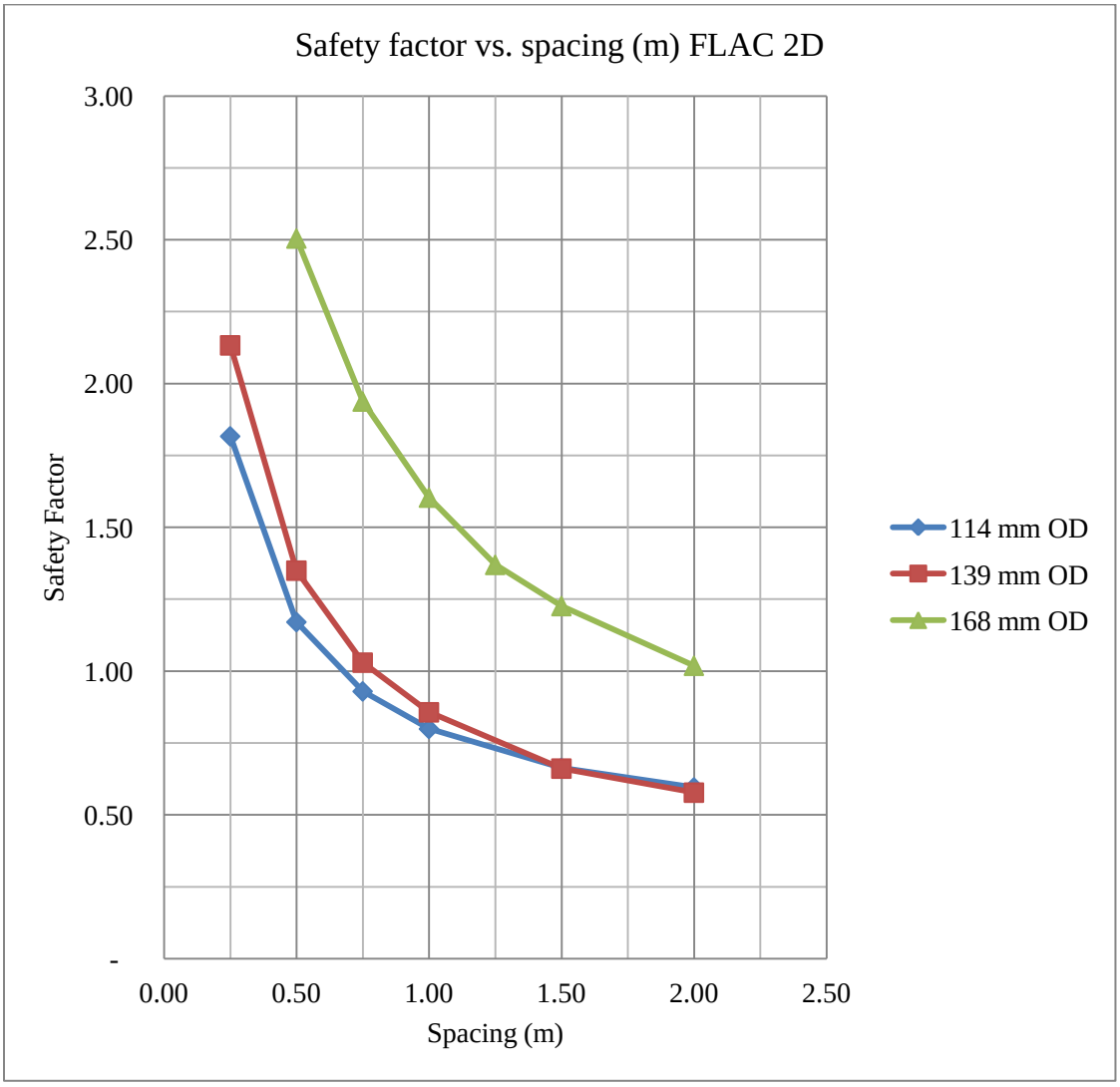

FIGURE 5.13 Safety factor vs. spacing plot for FLAC2D model

Table 5.4 shows the results of the modeling exercise performed in FLAC 3D for System 1. Again, the maximum bending stress and safety factor for each spacing and pipe geometry configuration are shown. The results for the FLAC 3D model are very similar to those produced by the FLAC 2D model. Any slight differences in results between the 2D and 3D analyses are due to the assumptions of the beam elements.The beam spacing in 3D is an actual physical characteristic of the model geometry.

Figure 5.14 depicts the results of the safety factor calculation graphically, where spacing is on the x-axis and safety factor is on the y-axis. Notice that the values of the safety factors are very similar to those produced by the FLAC 2D model, as expected. From this plot, a designer of System 1 can select a pipe diameter and a design criterion for an acceptable safety factor to get the proper spacing.

TABLE 5.4 Bending stress and safety factors for FLAC 3D model

Spacing (m)	Bending Stress FLAC 3D (MPa)			Safety Factor FLAC 3D		
	114 mm	139 mm	168 mm	114 mm	139 mm	168 mm
0.25	430.76	311.97	264.67	1.63	2.24	2.64
0.50	594.11	480.40	384.81	1.18	1.46	1.82
0.75	813.55	657.66	451.63	0.86	1.06	1.55
1.00	919.26	848.60	547.15	0.76	0.82	1.28
1.50	1,094.70	978.25	592.37	0.64	0.72	1.18

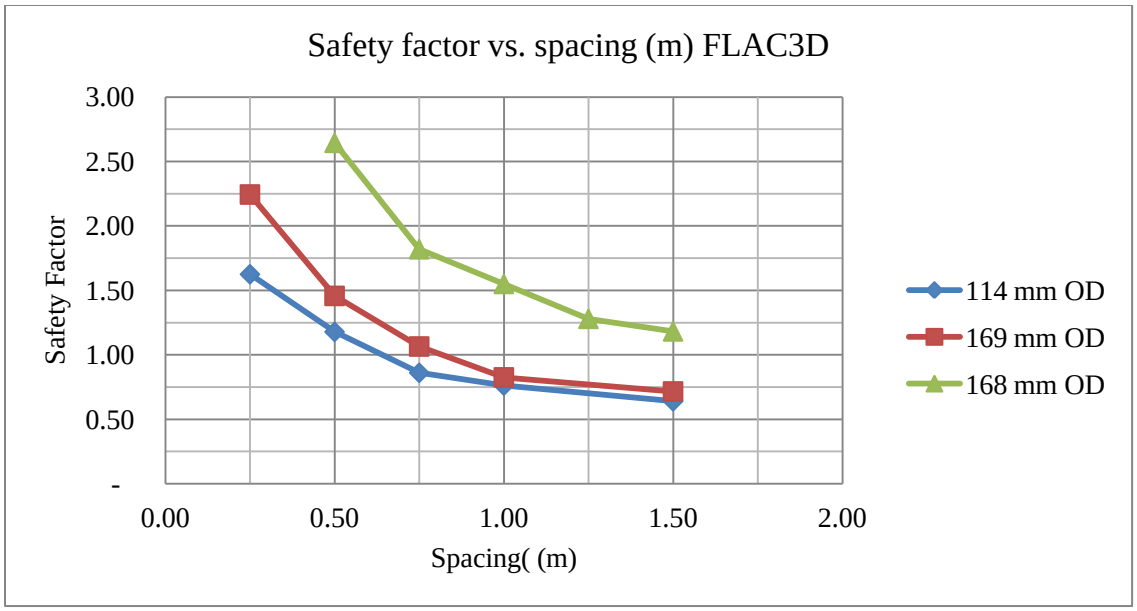

FIGURE 5.14 Safety factor vs. spacing plot for FLAC 3D model

5.6 Comparison of Analytical Calculations and FLAC Models for System 1

Results from the FLAC models of System 1 and the analytical calculations for the same system are compared in this section. Plotting the safety factor against the uniform spacing between pipes is the best way to directly compare the results. In addition to the results shown the analytical calculation section, more analyses were performed for assumed yield heights of 2 m and 3 m above the pipe umbrella system for each pipe and spacing configuration. Figures 5.15 through 5.17 show the comparisons between the FLAC 2D, FLAC 3D, and analytical safety factor calculations for varying pipe and spacing configurations. Each plot shows a different diameter of pipe and compares the numerical results to the analytical results. Spacing between pipes can then be determined based on the casing type and desired safety factor.

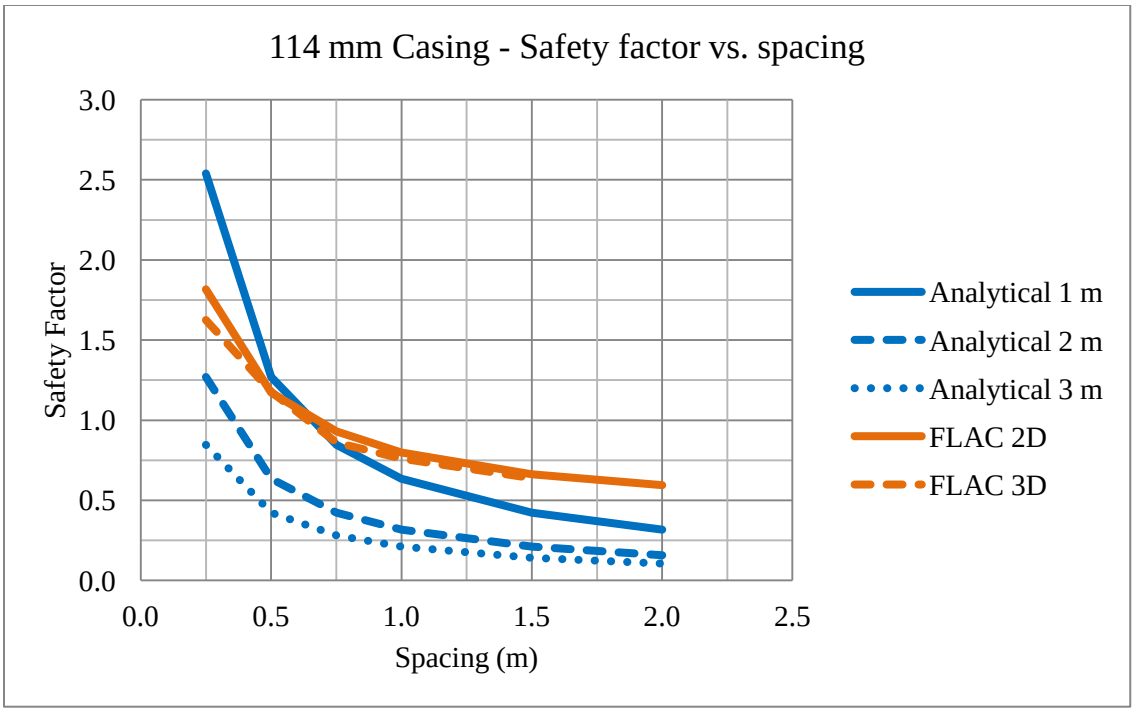

FIGURE 5.15 Safety factor vs. spacing comparison for 114 mm casing

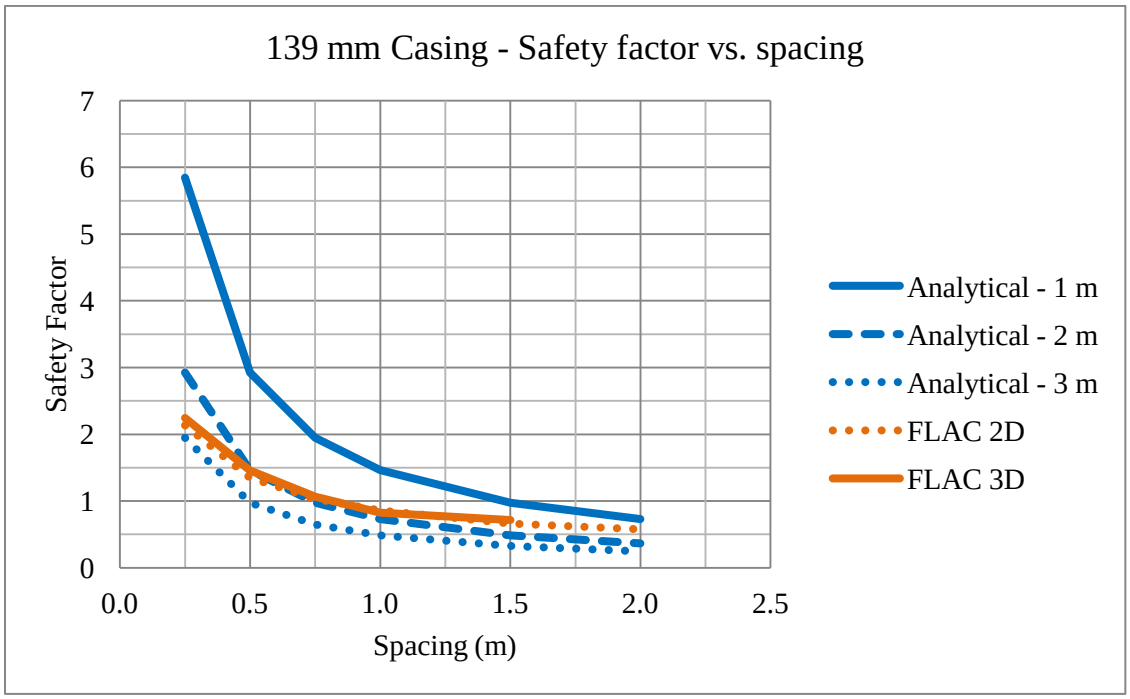

FIGURE 5.16 Safety factor vs. spacing comparison for 139 mm casing

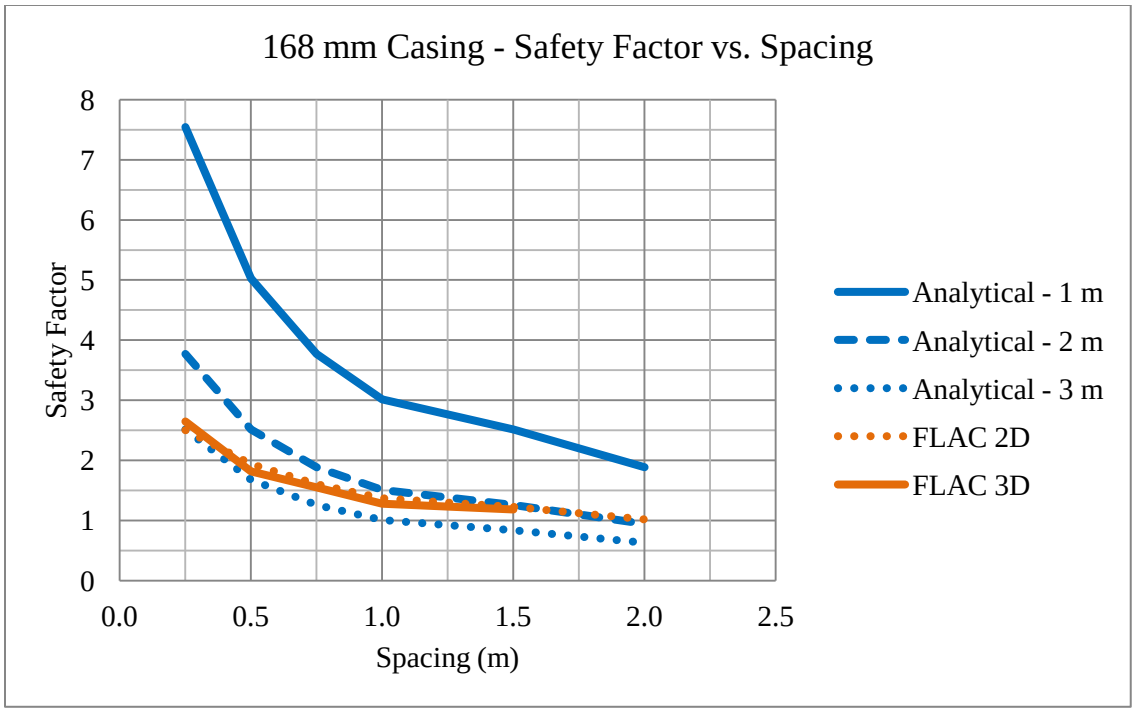

FIGURE 5.17 Safety factor vs. spacing comparison for 168 mm casing

Shown in the above figures, the results of the numerical simulations performed in FLAC 2D and 3D compare reasonably well with the analytical calculations. The analytical calculations make three assumptions of failure loads: 1 m, 2 m, and 3 m yield zones above the pipe umbrella system within the range of values that Terzaghi (1946) suggested for a tunnel of similar dimensions. For the numerical simulations performed in FLAC, a failure zone above the pipe umbrella (beam elements) was not assumed; rather it was developed in the finite difference grid due to the excavation. As long as the safety factors from the numerical simulations fall within the upper and lower limits (1 m and 3 m yield heights above pipe umbrella) then the FLAC results are valid.

One might argue that the analytical solutions are a more conservative approach to the design of such a system if the curve showing the lowest safety factor is selected. While this is true, the numerical simulations are much more rigorous and a more accurate

result would come from the FLAC model. For the 139 mm and 168 mm casing, the safety factors match the analytical calculations on the more conservative end.

The FLAC results for the 114 mm casing do not seem to match particularly well when the safety factor is less than 1. A safety factor of 1.5 is not even reached with the analytical method for yield heights of 2 m and 3 m above the pipe umbrella. It is reached, however, for a yield height of 1 m and with the FLAC 2D and 3D models where the spacing is between 0.25 and 0.5 m. Since the results of the 114 mm casing are quite variable between the analytical and numerical methods, the recommendation would be to have pipes spaced at least 0.25 m if a 114 mm diameter is used. For any configuration of pipe umbrella over a single entry, the author would not recommend a spacing over 1.0 m be used. The weak material in the roof will tend to fracture and fail between the pipes, so a relatively close spacing between umbrella pipes is desired. The recommendation is that if one has access and knowledge of a numerical modeling package, such as FLAC 2D or 3D, this methodology should be used. If this luxury is not available, the analytical solutions for the worst case scenario, i.e., largest assumed failure body above the pipe umbrella zone should be used. In the presented case, the largest assumed failure body was 3 m above the umbrella pipes; this will vary from site to site.

5.7 System 2: Pipe Umbrella Over Longwall Recovery Room – FLAC 3D

The conceptual model presented earlier for a directionally drilled pipe mesh over a longwall recovery room is a rather complex situation that could not be accurately modeled in two dimensions and capture the proper behavior of the mining process, stresses, strains, and displacements near the recovery room. Therefore a three-

dimensional model was created to simulate the ending section of a longwall panel as the mining progression approaches the longwall recovery room

Overall dimensions of the FLAC 3D model were 264 m by 191 m by 143 m for length, width, and depth respectively. At the mine, the longwall panels have a width of approximately 213 m; only one half the width of the longwall panel was modeled due to conditions of symmetry. Development sections of the western U.S. coal mine have entry and cross-cut dimensions of approximately 6 m by 4 m for width and height respectively. Pillar dimensions are approximately 52 m by 24 m for the larger pillars and 52 m by 18 m for the smaller yield pillars (closest to the longwall block on the headgate side). Figure 5.18 shows the extents of the FLAC 3D model with respect to the mine workings. Unlike the FLAC models for System 1, the model for System 2 extends from the surface elevation down to 28 m below the depth of the mined seam (D41). The D41 seam is at a depth of 111 m below the ground surface.

A total of 791,801 zones were employed in the model. The finite difference grid was discretized to 1 m by 1 m zones near the excavation and area of interest for the pipe umbrella mesh system and increase in size in the vertical and horizontal directions with greater distance from the gateroad section. The overall geometry of the outer boundaries of the FLAC 3D model for System 2 is shown in Figure 5.19. The color scale of the bulk modulus of each stratified layer assembled in the model is depicted in Figure 5.20. Important pieces of this diagram are pointed out, such as mining depth, location of channel sandstone, and location of the mined D41 coal seam.

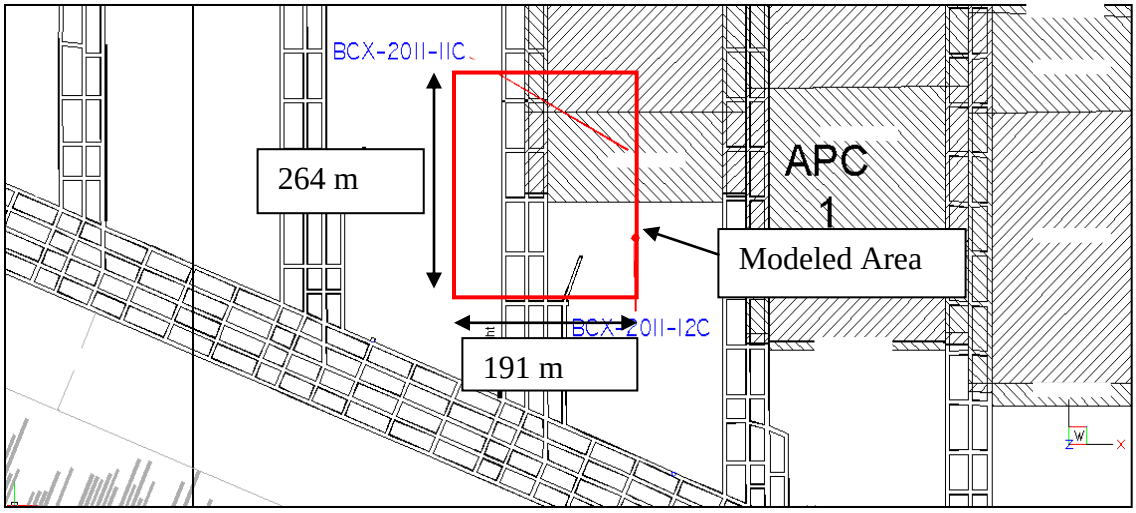

FIGURE 5.18 Extents of the FLAC 3D model with respect to the mine workings

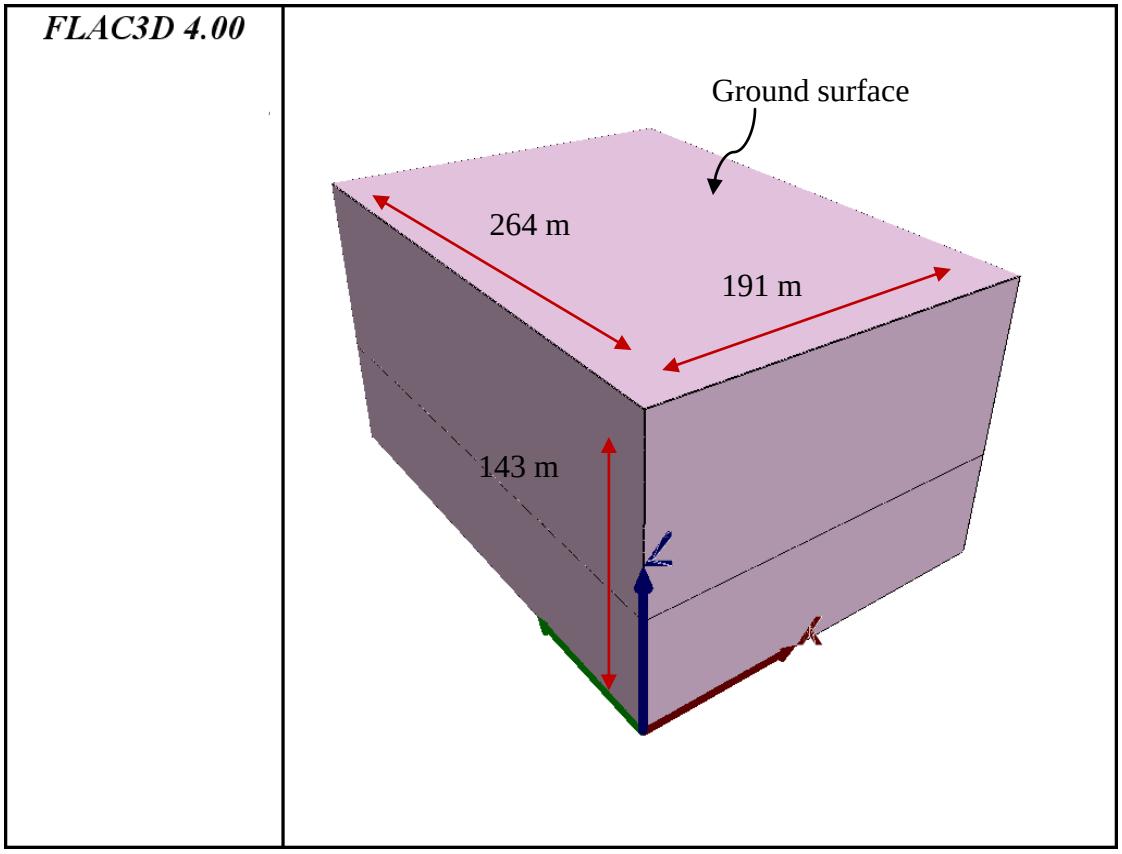

FIGURE 5.19 Overall dimensions of FLAC 3D model for System 2

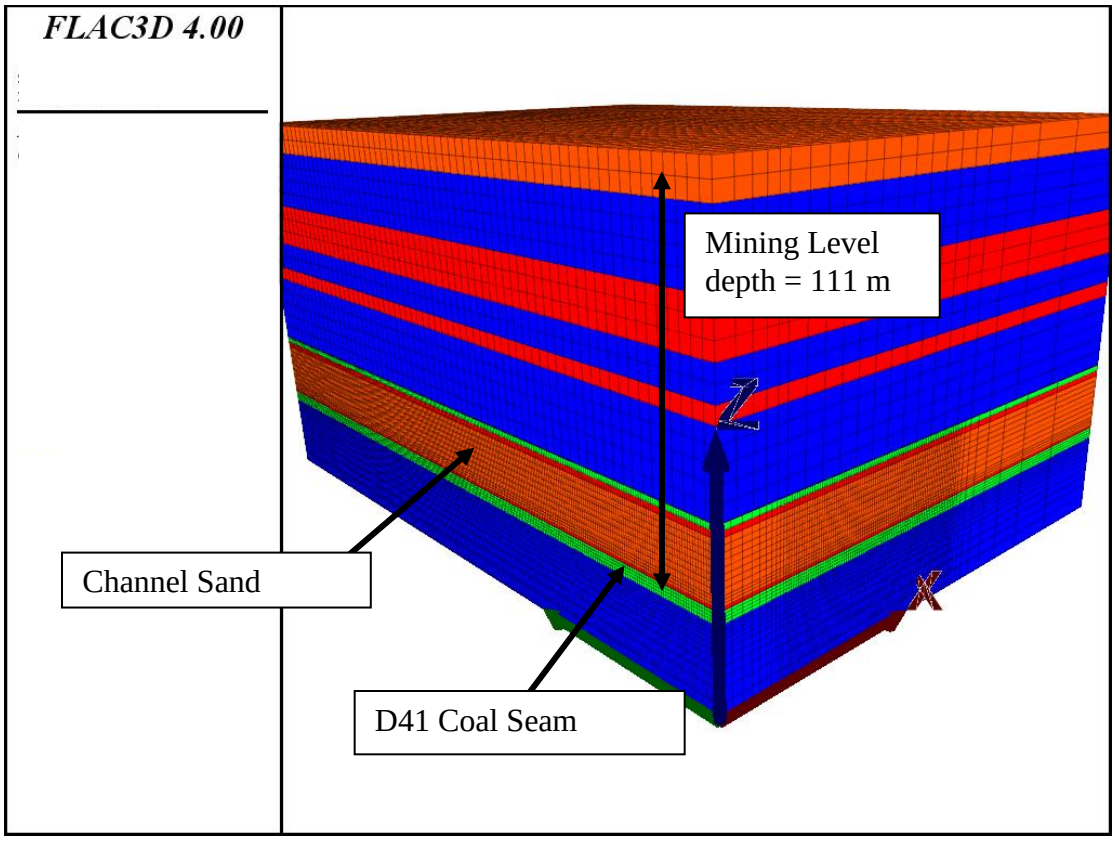

FIGURE 5.20 Color scale of the bulk modulus of the layers in the FLAC 3D model

The areas of extraction during the development and longwall mining process are depicted in Figure 5.21. The axes on the plot show the *X*, *Y*, and *Z* orientations of the coordinate system within the FLAC model. The *Y* direction in the FLAC model corresponds to due north in the field. The longwall mining process stops when the location of the recovery room is reached. The boundary of the grid ahead of the recovery room in the direction of mining was 1-1/2 pillar lengths. This facilitated the reduction of any end effects that the boundary of the model had on the stresses and displacements above the longwall recovery room.

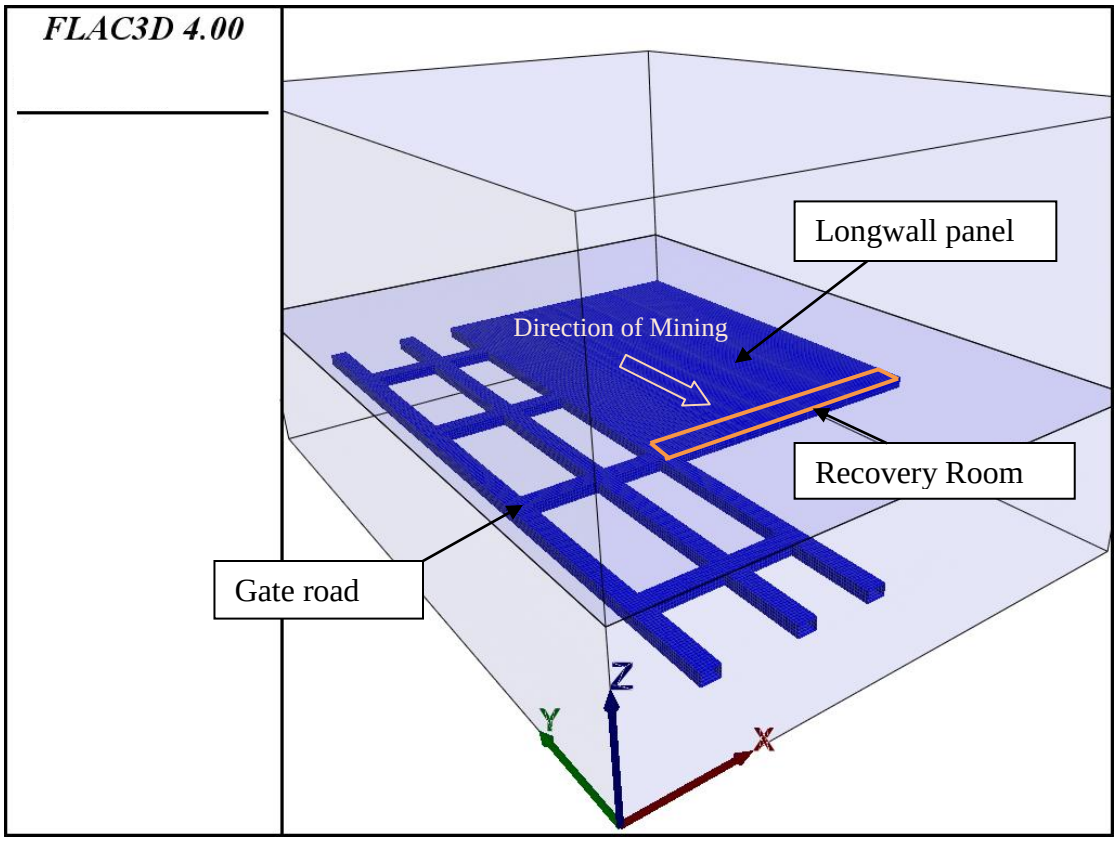

FIGURE 5.21 Geometry of excavated zones for FLAC 3D model of System 2

5.7.1 Boundary Conditions

Displacements normal to the sides and bottom of the mesh are not allowed; they are fixed at zero. The top surface is free to move as mining/excavation occurs at the D41 seam level. No external stresses were applied to the model boundaries, as a condition of gravity loading is assumed. When initial conditions are applied, the fixed boundaries allow the model to be in a state of equilibrium before any excavation takes place.

5.7.2 Initial Conditions

Initial conditions are essentially the boundary conditions in time. These are the stresses at the start of the excavation stage. The initial stress state for vertical stress is

from gravity loading only ($\sigma_v = \gamma h$). Horizontal stresses are estimated based on the vertical stress at depth and the component of tectonic stress based on the elastic modulus of the material at depth. A gravitational constant of 9.81 m/s^2 was assumed during the modeling process.

5.7.3 Modeling the Reinforced Zone

In a methodology proposed by Hoek (2000), modelling of the pipe mesh system was performed by calculating an equivalent stiffness of a composite material made up of three components: steel casing, grout (Portland cement), and the surrounding sandstone channel material. A composite elastic modulus was calculated based on an area weighted average. Figure 5.22 shows a cut away and cross section of the area reinforced by the pipe mesh.

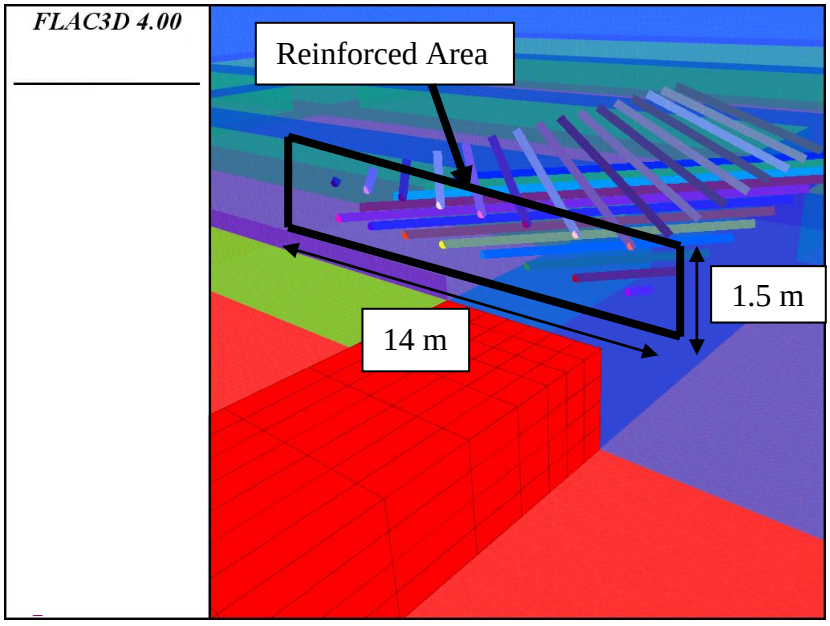

FIGURE 5.22 Cross section of the reinforced zone

The area that each component contributes to the composite is the projection on to the cross sectional face as shown above in Figure 5.22. The steel casing has an outer diameter of 114.3 mm and an inner diameter of 101.6 mm. The grout is considered to be a Portland cement water mix and fills the entire inner diameter of the steel casing. In this geometry the steel casing umbrella is spaced at approximately 2 m horizontally, and 1.5 m vertically. The overall dimensions of the reinforced zone are 14 m by 50 m by 1.5 m extending from the headgate into the longwall panel at a height of 2.5 m above the recovery room. Assumed elastic moduli of the three materials are presented in Table 5.5.

As stated earlier, the equivalent elastic modulus of the reinforced zone was calculated based on a weighted area average using the contributing area of each material projected on to a plane. Table 5.6 shows the calculation steps used to find the equivalent modulus of the reinforced area. Note that the equivalent modulus is approximately 185% of the modulus of the virgin rock. As expected, addition of a steel pipe umbrella and grout increases the overall stiffness of its zone of influence.

TABLE 5.5 Assumed elastic moduli for steel casing, grout, and surrounding rock

Material	Type	Elastic Modulus (GPa)
Steel Casing	A514	215
Grout	Portland Cement (1:1 mix)	27.5
Rock	Sandstone Channel	0.579

TABLE 5.6 Equivalent modulus calculation for reinforced zone

Material	Contributing Area, A (mm^2)	Elastic Modulus, E (GPa)	A * E (GPa-mm^2)
Steel Casing	34,456	215	6,891,222
Grout	129,717	27.5	3,567,221
Rock	20,835,827	0.579	12,063,944
Equivalent Modulus, E_{eq} (GPa)		1.072	

5.7.4 Modeling the Gob

Gob compaction is an important part of the longwall mining process, as it can alter the abutment stresses acting on adjacent pillars. Following undermining of the coal seam, the strata above fractures and forms a rubble zone, known as the gob, which behaves as a strain hardening material. Within the FLAC3D model, the programming language FISH was used to write a custom function which served as the method for "hardening" the gob material with increased vertical strain. Badr et al. (2003) suggested that an algorithm for "modulus updating" can be used to simulate the gob mass as it undergoes increased stresses and vertical strains:

$$K = \frac{1.75}{0.5 - \varepsilon_v} \text{ (MPa)} \tag{5.15}$$

where K = bulk modulus

ε_v = vertical strain in the particular zone

The height of caved material due to longwall mining was calculated using the following formula (Whittles et al. 2006):

$$H_c = \frac{100h}{C_1 h + C_2} \quad (5.16)$$

where H_c = caving height (m)

h = mining height (m)

C_1 and C_2 = empirically derived coefficients depending on stratum lithology (Table 5.7)

Assuming an average extraction height of 4 m and the lithology corresponding to soft and weak, the height of the caved zone was calculated to be approximately 7 m. In the FLAC3D model, the addition of the gob was performed by extracting the mined out area and the height of the gob above the mining horizon and replacing it with the strain hardening gob material. Figure 5.23 shows the extent of the gob zone within the FLAC 3D model.

5.7.1 System 2 FLAC 3D Model Results

The results of the FLAC 3D modeling for System 2 are presented in this section. A different approach for looking at the pipe umbrella system was used as compared to the modeling performed for System 1. As shown earlier, the reinforced zone was not modeled with beam elements. Rather, it was modeled by inserting a reinforced zone into the model that represents an equivalent stiffness of steel, grout, and the surrounding rock.

TABLE 5.7 Empirically derived coefficients for various stratum lithologies

Strata Type	C_1	C_2
Strong and hard	2.1	16
Medium strong	4.7	19
Soft and weak	6.2	32

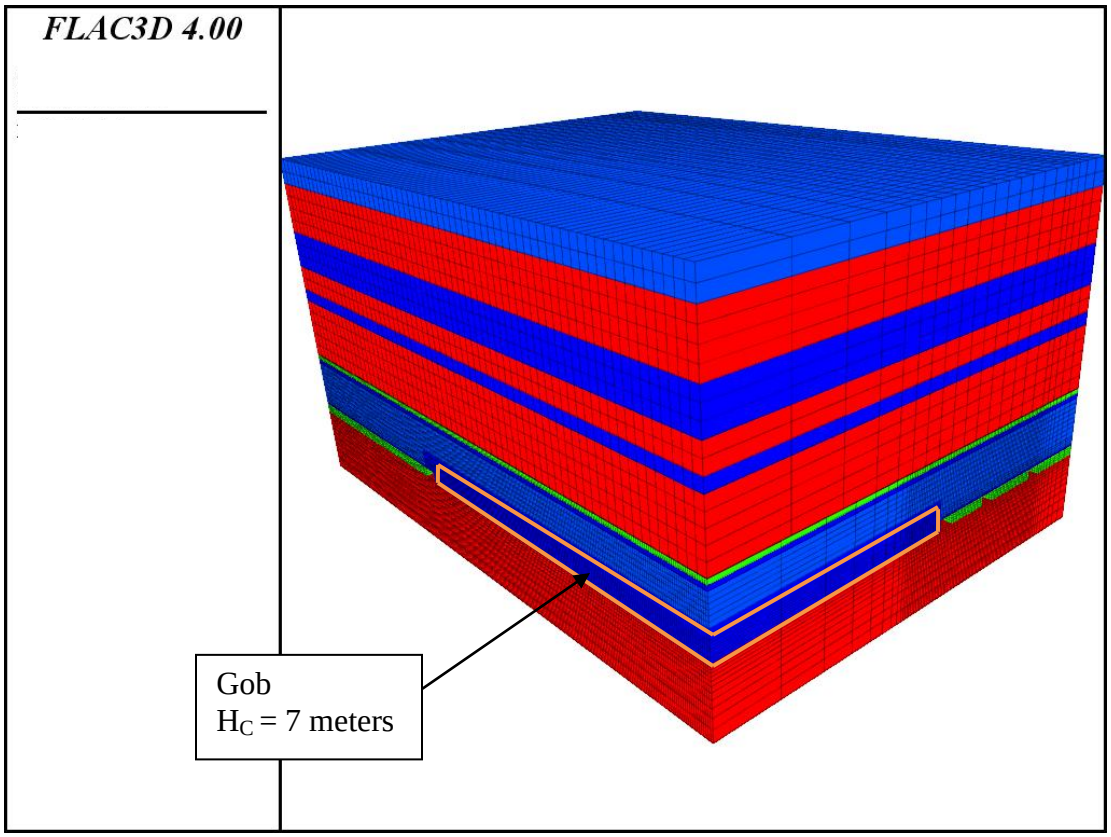

FIGURE 5.23 Extent of gob zone as employed in the FLAC 3D model

The approach taken in this analysis was to look at the effects of the displacement in the roof of the longwall recovery room. In FLAC 3D, System 2 was modeled for two cases (reinforcement and no reinforcement) and the displacements in the roof of the longwall recovery room were monitored. Figures 5.24 and 5.25 show profiles (in the direction of the long axis of the longwall panel) of displacement across the recovery room. Figure 5.24 shows the roof displacement to have a maximum of approximately 0.325 m relative to its original profile. Figure 5.25 shows the roof displacement to have a maximum of approximately 0.2 m. The dotted lines in the figures show the original roof profile.

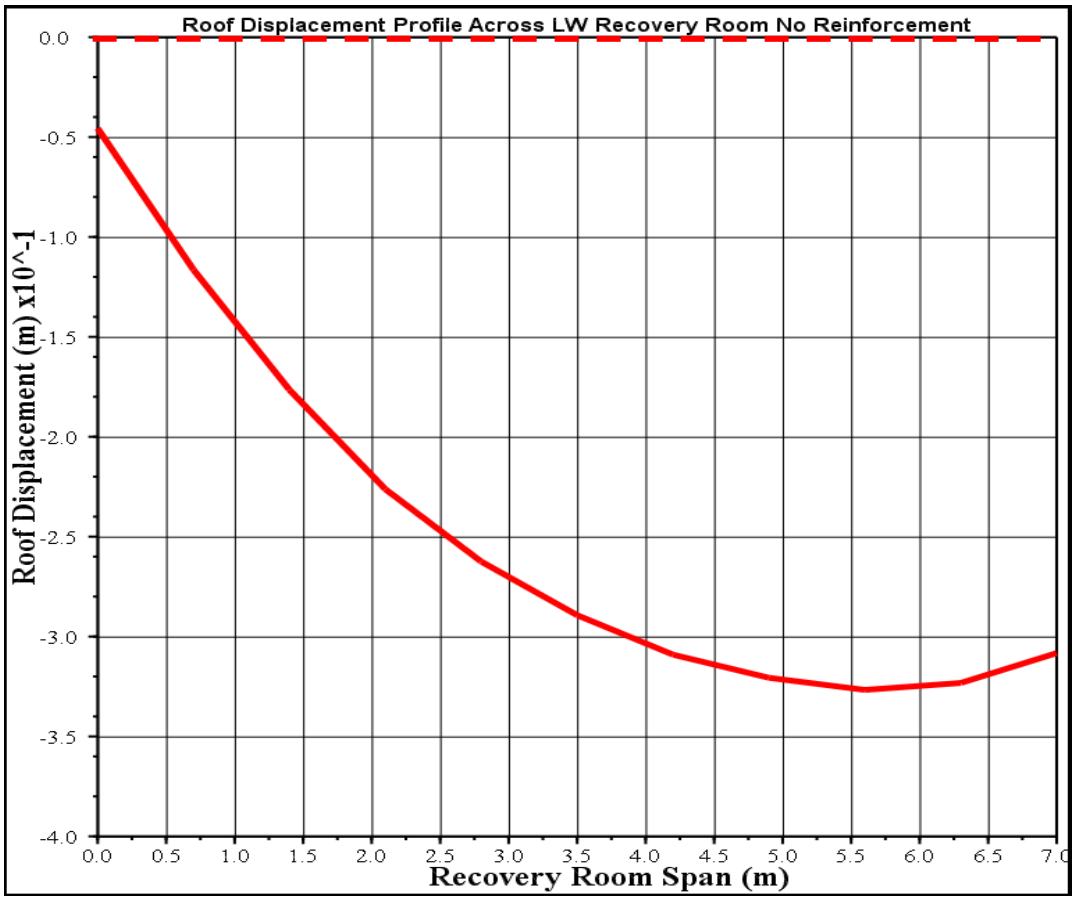

FIGURE 5.24 Roof displacement in the recovery room without reinforcement

The effect that the reinforced zone has is quite significant. In the FLAC model, the elastic modulus of the reinforced zone was increased by 185% (compared to the virgin rock) and the results show that the displacements in the roof are reduced by approximately 0.125 m. If a double-layered pipe umbrella mesh is installed in the immediate roof of the longwall recovery room, it can be concluded that System 2 will have a beneficial effect on the longwall shield recovery process.

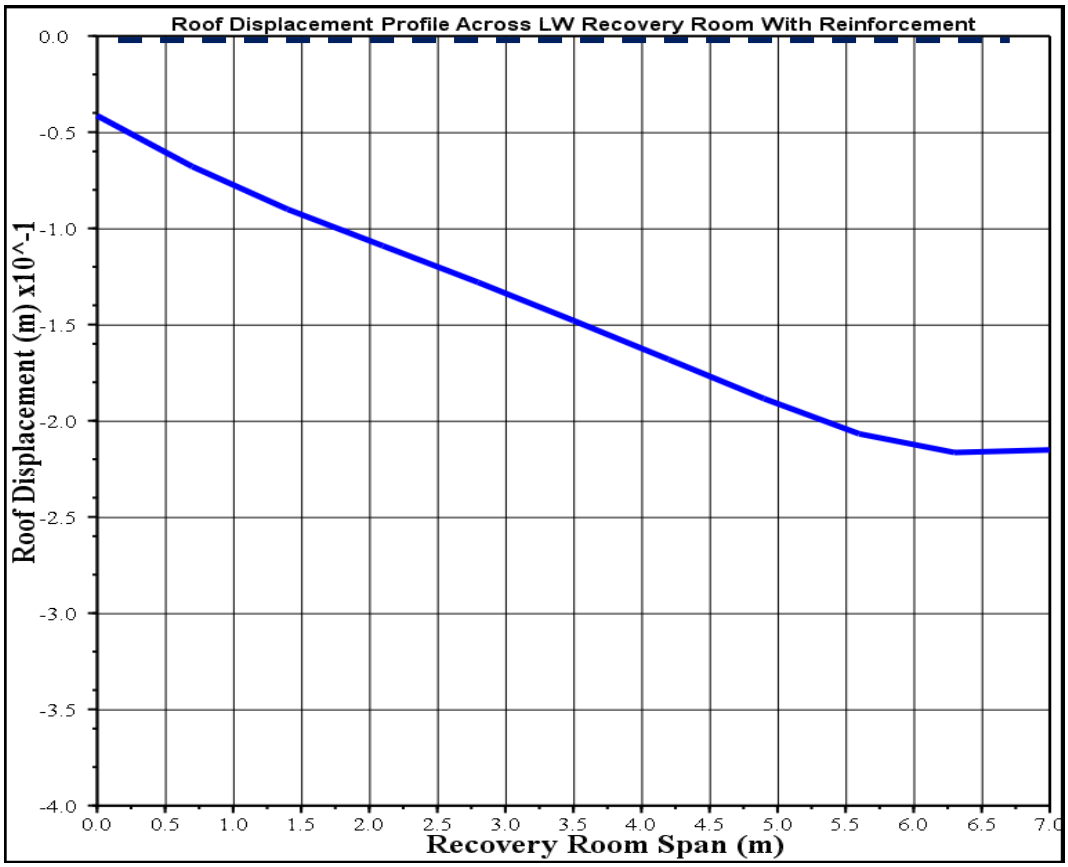

FIGURE 5.25 Roof displacement in the recovery room with reinforcement

5.7.2 Validation of the 3D Model

The extraction of coal in a longwall panel leads to the redistribution of stress of the in-situ vertical stress into the strata of the adjacent and unexcavated portions of the mining horizon. Zones closer, relatively, to the mined out panel will experience the greatest amount of increase in vertical stress due to under mining. This increase in vertical stress decays with increasing distance from the mined out areas. The increase in stress is commonly referred to as the abutment stress. Immediately adjacent to the mined out longwall panel, the concentrated vertical loads lead to material failure and yield zone development (Whittles et al., 2005). In the absence of actual field stress and displacement measurements taken in the rock strata, the vertical stress distribution due to undermining

from the FLAC 3D model was compared to an established empirical model developed to estimate the vertical stress pattern around a longwall panel proposed by Wilson.

According to Wilson, the mathematical model of the decrease in vertical stress at increasing distance from the longwall face can be described by the following:

$$\sigma = (\hat{\sigma} - q)e^{\left(\frac{x_b - x}{c}\right)} + q \tag{5.17}$$

$$c = \frac{0.15H - {}^{M}/_{2}}{(k-1)+40\frac{\sigma_0}{H}} \tag{5.18}$$

$$k = \frac{\sigma_h}{\sigma_v} \tag{5.19}$$

$$\hat{\sigma} = kq + \sigma_0 \tag{5.20}$$

where q = vertical stress due to weight of overburden (MPa)

x_b = yield zone (m)

x = distance from longwall face (m)

c = exponential decay factor

H = mining depth (m)

W = panel width (m)

k = triaxial stress factor (ratio of horizontal stress to vertical stress at depth)

m = extraction height (m)

σ_0 = unconfined compressive strength of the coal

For the geometry of the present problem, the parameters shown in Table 5.8 were calculated and used in the Wilson model. Figure 5.26 shows the results of the model validation. The data presented in the figure show reasonable agreement between Wilson's

TABLE 5.8 Parameters used in the Wilson model

H (m)	M (m)	k	q (MPa)	(MPa)	c	σ_0 (MPa)	x_b (m)
111	4	~1.2	2.74	7.05	9.41	3.76	1.89

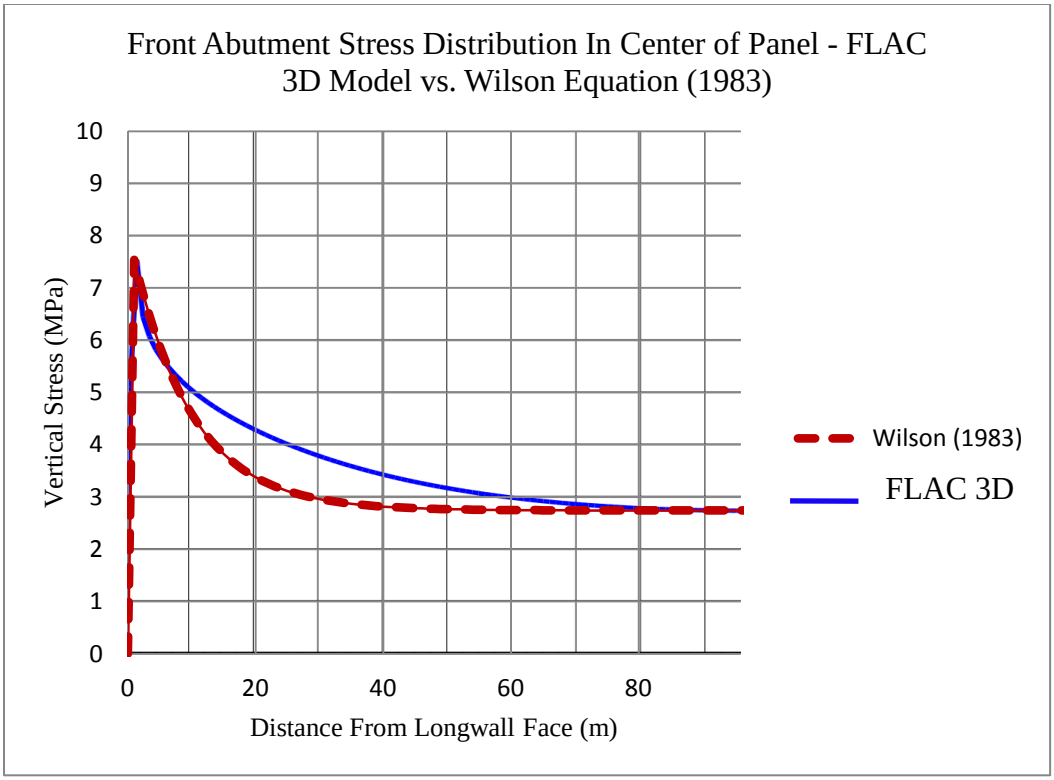

FIGURE 5.26 Front abutment stress distribution for the FLAC 3D model

method and the FLAC3D model. Both models predict the same maximum abutment stress of about 7.5 MPa with a yield zone of approximately 2 m. The vertical stress decays to reach the same in-situ vertical stress at approximately 80 m from the longwall face. However, the Wilson model shows a faster rate of decay in vertical stress with increased distance from the longwall face than the FLAC3D model. It can be concluded that the numerical model produced satisfactory results and predicts the correct behavior.

Figure 5.27 shows a vertical stress contour plot along with an abutment stress profile along the center line of the long axis of the panel. The location of the simulated strain-hardening gob material is also depicted. As shown, a sharp increase in vertical stress is present just inby the recovery room. With increased distance into the gob, the vertical stress begins to increase as gob compaction has occurred within the numerical model. The FLAC 3D model was also validated against actual field data supplied from the western U.S. coal mine for subsidence. A subsidence profile for the particular longwall panel was constructed from these data and compared to the vertical displacement profile generated from the FLAC 3D model. The results of this analysis are presented in Figure 5.28.

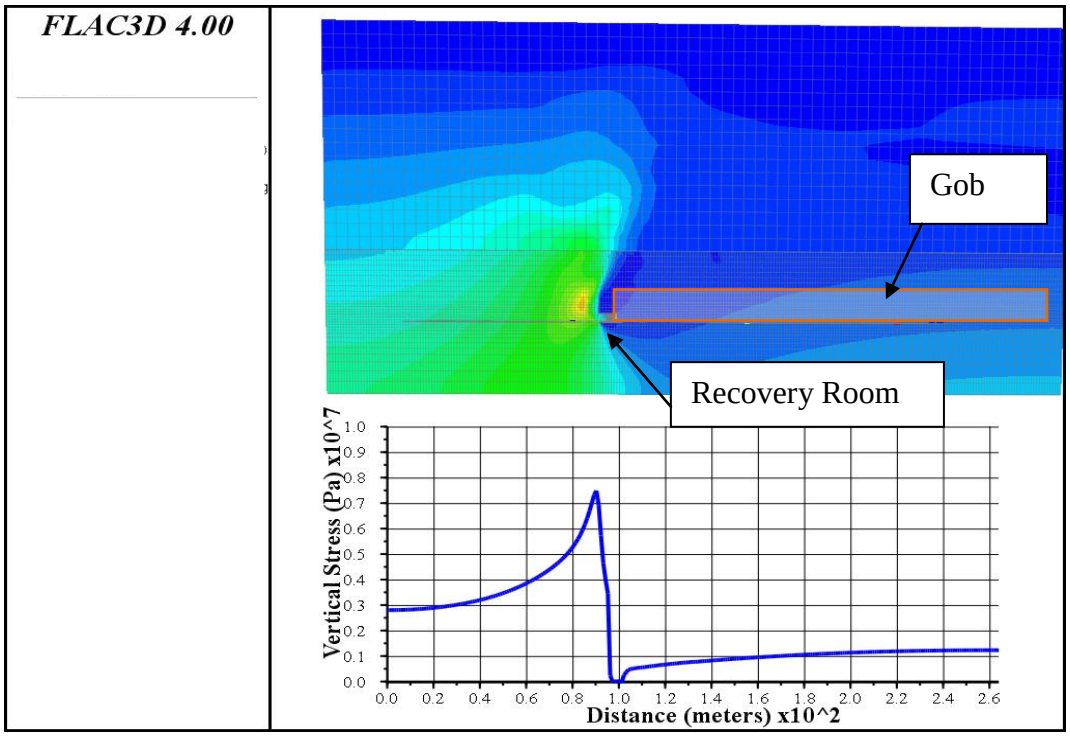

FIGURE 5.27 Vertical stress contour plot along the center line of the longwall panel

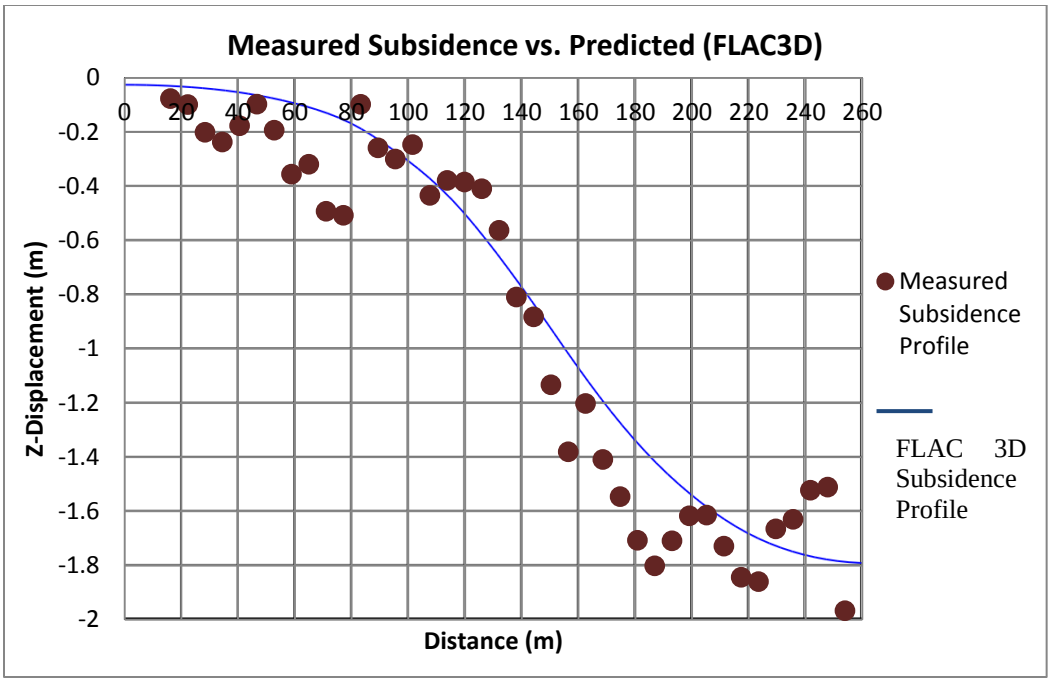

FIGURE 5.28 Measured subsidence vs. predicted subsidence from FLAC 3D

The predicted subsidence profile from the FLAC 3D model agrees very well with those values taken from field measurements. This particular subsidence profile is the vertical displacement ahead of the longwall face, parallel to the longwall mining direction. Measured values at each distance were determined from a contour map of the subsidence profile overlaid on the mine workings.

By performing the validation exercises, the numerical model is proven to be an accurate representation of the field situation. From this, one can conclude that the overall behavior and results of the presented FLAC 3D model are true. A model is valid only if the results can be compared to its real world situation and the key aspects of the actual situation are evident in the numerical model. Thus, it can be concluded that if the roof of a longwall recovery room were reinforced with a double layered pipe umbrella mesh, the displacements in the roof would be reduced. Magnitudes of displacement reduction

would, of course, vary by site location. In general terms, a pipe umbrella system above a longwall recovery room would most definitely aid in the roof control of such an excavation.

6 CONCLUSION

Weak roof conditions in underground coal mines are very common and can cause significant delay during production. In longwall coal mining, poor ground conditions can cause unplanned delay during the longwall shield recovery process due to excessive closure or failure in the roof of a recovery room near the headgate and tailgate ends of the panel. Mine operators must look into alternative roof support methods which reinforce current day to day practices. Two methods of ground reinforcement were presented in this paper.

The first (System 1) is a pipe umbrella system over a single mine entry. This method involves the installation of drill casing into boreholes drilled from an adjacent entry or travel way. The second (System 2) is a double layered pipe umbrella mesh over a longwall recovery room. The idea behind System 2 is that it can be installed as a method of pre-support above a future longwall recovery room. State of the art technologies in horizontal directional drilling must be used for precision borehole placement.

A case study was performed for the implementation of both System 1 and System 2 at a particular western U.S. coal mine. Laboratory tests were performed on a weak channel sandstone that exists the roof of this mine. Unconfined compressive strength (UCS), tensile strength, and Young's Modulus were found through testing performed at the University of Utah. The Unconfined compressive strength was found to be 11.07 MPa as the average of 14 samples tested in the laboratory. Tensile strength was found to be

0.523 as the average of 32 samples using the Brazilian test. Young's modulus was found to be 3.63 GPa as the average of 14 samples. Results of the laboratory testing showed consistency with historical geotechnical data of the same formation. This laboratory testing information was used as input in to the FLAC 2D and 3D models.

Numerical modeling in the commercial finite difference software packages FLAC 2D and FLAC 3D was performed for three separate models. The first model was two-dimensional and simulates the excavation of a typical three entry gate road section in the western U.S. coal mine for System 1. Beam elements were installed in the model above one of the mine entries and the spacing was varied in the out-of-plane direction along with the geometric parameters. The purpose of this model was to determine the bending stress in a pipe umbrella due to undermining. The second model was three-dimensional simulation of System 1. Results for the safety factor of the beams in first and second models are compared against an analytical calculation of a beam in bending with a uniformly distributed load.

An analysis of design for pipe umbrella roof support was performed based on the results of the numerical modeling. Beam elements in FLAC 2D and 3D undergo bending due to undermining and develop moments. Using well-known beam bending formulas, a factor of safety was determined for various configurations of an umbrella pipe system over a single coal mine entry. The results of the numerical modeling were also compared to an analytical model that assumes a bending beam with fixed ends and a uniformly distributed load. A failure body that the pipes must hold up was assumed to be on the range of 1.5 m to 3.0 m above the pipe umbrella. Results of the FLAC models and analytical model showed close correlation.

The third model is a three-dimensional simulation of a recovery room as longwall mining approaches the end of a panel for System 2. A reinforced zone was installed in the immediate roof above the recovery room and the stresses and displacements were monitored. The results show that a relative increase in stiffness of about 185% for a reinforced zone reduce the displacements in the longwall recovery room roof by approximately 0.125 m (5 in.). This is a substantial amount, as it pertains to such a small area in a very large numerical model. A reduction in roof displacement after longwall shield recovery would be extremely beneficial to mine operators who struggle with delay during this process. Numerical modeling of the reinforced roof above a longwall recovery room shows that a reduction in closure can be achieved. Validation of the FLAC 3D model was performed against field subsidence data and established empirical formulas.

Geotechnical conditions of a particular western U.S. mine were used in all of the analyses. Material properties from laboratory testing performed at the University of Utah and other sources were used in the numerical models. Although this research is focused on a specific western U.S. mine, the methods proposed in this paper can be applied to coal mines in general. The research shows that pipe umbrella systems can be utilized in the coal mine setting where weak roof conditions exist. The effectiveness of a carefully designed pipe umbrella system is controlled by the pipe spacing, strength of the steel, and the structural geometry of the pipe. For an acceptable design, the factor of safety based on the structural analysis of the steel should be at least 1.5 for support in an underground mine.

Based on the site specific analysis of the western U.S. coal mine performed, the spacing between parallel pipes over a coal mine entry should be on the range of 0.25 m to

1.0 m depending on the diameter of casing selected. A series of design plots showing the safety factor variance with pipe spacing were generated for the three most common types of high strength steel casing used for pipe umbrella systems (114 mm, 139 mm, and 168 mm diameter). It should be understood that the system is designed to only support the material above the pipe umbrella. While a pipe umbrella system might assist in the stability of roof bolts, its main purpose is to prevent catastrophic and continuous failure.

APPENDIX

TABLE A.1 Young's Modulus and UCS results for channel sandstone.

Sample ID	Length (in.)	Diameter (in.)	F_{max} (lbf)	C_0 (psi)	C_0 (MPa)	Ks (lbf/in.)	Kt (lbf/in.)	Kr (lbf/in.)	E (GPa)
BCC-29-C2	4.936	2.365	5331.93	1,213.8	8.369	5,525,646.15	393,217.26	423343.3108	3.279
BCC-29-C6	5.059	2.382	4952.93	1,111.4	7.663	5,525,646.15	516,832.15	570161.2357	4.462
BCC-29-C8	4.969	2.386	7985.73	1,786.0	12.314	5,525,646.15	424,400.60	459708.8139	3.522
BCC-29-C9	4.888	2.388	7520.62	1,679.9	11.582	5,525,646.15	387,004.29	416150.5751	3.132
BCC-29-C10	5.043	2.373	6175.00	1,396.2	9.627	5,525,646.15	388,489.36	417868.2536	3.285
BCC-32-C11	5.045	2.389	8488.94	1,893.8	13.057	5,525,646.15	501,342.93	551368.7191	4.278
BCC-32-C13	5.000	2.395	6243.49	1,385.9	9.555	5,525,646.15	377,163.96	404793.9774	3.098
BCC-32-C15	4.938	2.365	7929.66	1,805.1	12.446	5,525,646.15	439,435.34	477401.4065	3.700
BCC-32-C18	4.980	2.385	8375.47	1,874.7	12.926	5,525,646.15	452,752.15	493159.9546	3.790
BCC-32-C20	4.969	2.379	7139.12	1,606.7	11.078	5,525,646.15	406,798.35	439126.8942	3.386
BCC-34-C27	4.958	2.382	8340.18	1,871.6	12.904	5,525,646.15	446,743.03	486038.7854	3.728
BCC-34-C28	5.016	2.390	8823.41	1,966.8	13.560	5,525,646.15	524,145.96	579075.2766	4.464
BCC-34-C30	5.013	2.386	6837.21	1,529.1	10.543	5,525,646.15	404,139.47	436030.2243	3.370
BCC-34-C33	5.059	2.375	5979.90	1,349.8	9.307	5,525,646.15	391,083.16	420870.7073	3.313

TABLE A.2 Brazilian test results for channel sandstone

Specimen No.	Depth (ft)	D (in)	t (in)	Weight (lbf)	Density (lbf/ft^3)	$P_{initial}$ (lbf)	P_{final} (lb)	s_t (psi)
D1	300.38	2.3640	1.032	0.329	125.650	0.000	230	60.02
D2	300.46	2.3450	1.033	0.335	129.621	0.000	275	72.27
D3	300.54	2.3600	1.017	0.333	129.306	0.000	225	59.68
D4	302.69	2.3800	1.080	0.346	124.324	32.000	327	73.06
D5	302.77	2.3800	1.070	0.338	122.605	32.000	236	51.00
D6	303.52	2.3900	1.090	0.352	124.259	32.000	277	59.87
D7	304.66	2.3600	1.030	0.346	132.748	32.000	298	69.66
D8	304.74	2.3800	1.030	0.339	127.949	32.000	312	72.71
D9	305.59	2.3700	1.080	0.348	126.095	32.000	259	56.46
D10	306.38	2.3600	1.070	0.348	128.355	32.000	268	59.50
D11	306.46	2.3790	1.065	0.344	125.699	32.000	257	56.54
D12	306.54	2.3790	1.066	0.343	125.018	32.000	316	71.29
D13	329.99	2.3930	1.059	0.363	131.815	32.000	386	88.93
D14	330.60	2.3900	1.037	0.348	129.217	31.000	254	57.28
D15	330.68	2.3980	1.031	0.348	129.104	31.000	297	68.49
D16	330.76	2.3895	1.041	0.346	128.040	31.000	305	70.13
D17	336.44	2.3810	1.020	0.340	129.271	31.000	265	61.34
D18	336.52	2.3765	1.025	0.337	127.946	31.000	321	75.79
D19	336.60	2.3680	1.016	0.331	127.701	31.000	303	71.97
D20	336.78	2.3730	1.031	0.338	128.065	31.000	324	76.28
D21	337.51	2.3955	1.048	0.349	127.658	31.000	246	54.55
D22	337.59	2.3895	1.042	0.355	131.284	31.000	311	71.59
D23	337.67	2.3905	1.037	0.349	129.425	31.000	385	90.91
D24	337.75	2.3720	1.036	0.340	128.337	31.000	400	95.64
D25	338.73	2.3940	1.042	0.350	128.801	31.000	390	91.62
D26	338.81	2.3800	1.029	0.350	132.059	31.000	332	78.24
D27	349.90	2.4000	1.050	0.360	130.807	32.000	613	146.78
D28	351.17	2.3915	1.042	0.356	131.350	31.000	425	100.66
D29	351.25	2.3780	1.051	0.359	133.003	31.000	376	87.92
D30	351.33	2.3905	1.047	0.362	133.068	31.000	472	112.23
D31	351.41	2.3930	1.038	0.363	134.326	31.000	379	89.23
D32	352.75	2.3820	1.033	0.349	131.258	31.000	325	76.10

FLAC 3D Strain Hardening Model Code:

```
def calc_mod
array arr(6)
whilestepping
local pnt = zone_head
  loop while pnt # null
    if z_group(pnt) = 'gob' then
      dum = z_fsr(pnt,arr)
      z_extra(pnt,1) = z_extra(pnt,1) + abs(arr(3))
      z_extra(pnt,2) = abs(arr(3))
      tot_strain = abs(z_extra(pnt,1))
        if tot_strain < 0.5 then
          tot_strain = tot_strain
        else
          tot_strain = 0.499
        end_if
        z_extra(pnt,2) = tot_strain
        v = 0.30
        k = (1.75 / (0.5 - tot_strain)) * 1000000
        g = (3 * k * (1 - 2 * v)) / (2 * (1 + v))
        z_prop(pnt,'bulk') = k
        z_prop(pnt,'shear') = g
    else
      pnt = z_next(pnt)
    end_if
  pnt = z_next(pnt)
  endloop
end
```

REFERENCES

Advanced Terra Testing, Inc. 2004. *Unconfined Compressive Strength with Stress/Strain Measurements ASTM D 3148*. Laboratory measurements for Bridger Coal Company. Lakewood, CO: Geotechnical Laboratory.

Amorin, R., and Broni-Bediako, E. 2010. Application of minimum curvature method to wellpath calculations. *Research Journal of Applied Sciences, Engineering and Technology*. 2(7): 679-686.

ASTM Standard D 3967-08. 2008. *Standard Test Method for Splitting Tensile Strength of Intact Rock Core Specimens*. West Conshohocken, PA: ASTM International. Available from www.astm.org.

ASTM Standard D 7012-10. 2010. *Standard Test Method for Compressive Strength and Elastic Moduli of Intact Rock Core Specimens under Varying States of Stress and Temperatures*. West Conshohocken, PA: ASTM International. Available from www.astm.org.

Badr, S., Ozbay U., Kieffer S., and M. Salamon. 2003. Three-dimensional strain softening modeling of deep longwall coal mine layouts. *FLAC and Numerical Modeling in Geomechanics*. 3:233-239.

Barczak, T.M., and Tadolini, S.C. 2004. Design parameters of roof support systems for pre-driven longwall recovery rooms. In *Proceedings of 2004 SME Annual Meeting*, Denver CO, Feb 23-25. Littelton, CO: SME.

Brown, E.T., and Hoek, E. 2002. Practical estimates of rock mass strength. *International Journal of Rock Mechanics and Mining Sciences*. 34(8):1165-1186.

Curran, J.H., and Hammah, R.E. 2009. It is better to be approximately right than precisely wrong: why simple models work in mining geomechanics. In *Proceedings of 43rd US Rock Mechanics Symposium*, Asheville, NC, June 28-July 1. Alexandria, VA: ARMA.

Esterhuizen, E., Mark, C., and Murphy, M.M. 2010. Numerical model calibration for simulating coal pillars, gob and overburden response. In *Proceedings of the 29th International Conference on Ground Control in Mining*, Morgantown, WV, July 27-29. Morgantown, WV: West Virginia University.

Hasagawa, O., Lee, F.H., Shinji, M., Suzuki, H., Tan, S.E., and Yeo, C.H. 2009. Three dimensional numerical modeling of a NATM tunnel. In *International Journal of the JCRM*. 5(1):33-38.

Hibbeler, W.C. 2005. Deflection of beams and shafts. In *Mechanics of Materials*, 6th ed. Edited by M.J. Horton. Upper Saddle, NJ: Pearson Prentice Hall.

Hoek, E. 2000. Numerical modeling for shallow tunnels in weak rock. *Presented during the 5th GRC Lecture*, NTU, Singapore: Unpublished work.

Itasca Consulting Group. 2005. FLAC version 5.0. Users Manual. *Itasca Consulting Group, Inc*., Minneapolis, 2005.

Itasca Consulting Group. 2009. FLAC3D Version 4.0. Users Manual. *Itasca Consulting Group, Inc*., Minneapolis, 2009.

Jobling, S., Kingman, S.W., Lowndes, I.S., Whittles, D.N., and Yates, C. 2006. Influence of geotechnical factors on gas flow experienced in a uk longwall coal mine panel. *Int'l Journal of Rock Mechanics & Mining Sciences*. 43:369-387.

Larson, M.K., and Whyatt, J.K. 2009. Critical review of numerical stress analysis tools for deep coal longwall panels under strong strata. In *Proceedings of 2009 SME Annual Meeting*, Denver, CO, Feb 22-25. Littelton, CO: SME.

Maleki Technologies. 2003. Structural mine layout design progress review for the ten-mile rim. *Maleki Technologies, Inc. Consulting Mining & Geotechnical Engineers*. Spokane, WA.

Mark, C., and Molinda, G. 2010. Ground control failures in coal mines with weak roof. *Electron J Geotech Eng*. 15(F): 547-588.

NERCO, Inc. Technical Services Department. 1981. A preliminary report on the depositional framework of the Jim Bridger coal deposits special report 017. *Technical Services Department, NERCO, Inc*. Portland, OR.

NSA Geotechnical Services, Inc. 2003. Determination of secondary principal horizontal stresses at the bridger coal company property using the downhole overcoring method. Golden, CO: Geotechnical Services

Pariseau, W.G. 2006. *Design Analysis in Rock Mechanics*. AK Leiden, The Netherlands: Taylor & Francis.

Schubert, W., and Volkmann, G.M. 2008. Tender document specifications for pipe umbrella installation methods. In *World Tunnel Congress 2008*, Arga, India, Sept 22-24. New Delhi, India: ITA-AITES.

Tadolini, S.C. 2003. Ground control support considerations for pre-driven longwall recovery rooms. Ph.D. dissertation, West Virginia University, WV.

TerraTek. 2011. *Continuous Strength Profiling and Triaxial and Unconfined Compression Testing of Selected Core Material*. Laboratory measurement report for Bridger Coal Company. Salt Lake City, UT: Geotechnical Laboratory.

Terzaghi, K. 1946. Rock defects and loads on tunnel supports. In *Rock Tunneling with Steel Supports.* Edited by R.V. Proctor and T. White. Youngstown, Ohio: Commercial Shearing and Stamping Co. 15-99

Wilson, A.H. 1983. The stability of underground workings in the soft rocks of the coal measures. *International Journal of Mining Engineering.* 1:91-187

Vutukuri, V.S., Lama R.D., and Saluja, S.S. 1974. *Handbook on Mechanical Properties of Rocks*. Vol. 1, Clausthal, Germany: Trans Tech.